



P-glycoprotein deficient mouse *in situ* blood–brain barrier permeability and its prediction using an *in combo* PAMPA model[☆]

Claude Dagenais^{a,1}, Alex Avdeef^{b,*}, Oksana Tsinman^b, Adam Dudley^a, Richard Beliveau^c

^a AstraZeneca Pharmaceuticals, 1800 Concord Pike, Wilmington, DE 19850, USA

^b pION INC, 5 Constitution Way, Woburn, MA 01801, USA

^c Laboratoire de Médecine Moléculaire, Université du Québec à Montréal, C.P. 8888, Succursale Centre-Ville, Montréal, Québec, Canada H3C 3P8

ARTICLE INFO

Article history:

Received 20 February 2009

Accepted 25 June 2009

Available online 8 July 2009

Keywords:

Blood–brain barrier

mdr1a(–/–) mice *in situ* brain perfusion

Brain penetration classification (BPC)

P-glycoprotein

In combo PAMPA

ABSTRACT

The purpose of the study was to assess the permeability of mouse blood–brain barrier (BBB) to a diverse set of compounds in the absence of P-glycoprotein (Pgp) mediated efflux, to predict it using an *in combo* PAMPA model, and to explore its role in brain penetration classification (BPC). The initial brain uptake (K_{in}) of 19 compounds in both wild-type and Pgp mutant [mdr1a(–/–)] CF-1 mice was determined by the *in situ* brain perfusion technique. PAMPA measurements were performed, and the values were used to develop an *in combo* model, including Abraham descriptors. Published rodent K_{in} values were used to enhance the dataset and validate the model. The model predicted 92% of the variance of the training set permeability. In all, 182 K_{in} values were considered in this study, spanning four log orders of magnitude and where Pgp decreased brain uptake by as much as 14-fold. The calculated permeability–surface area (PS) values along with literature reported brain tissue binding were used to group molecules in terms of their brain penetration classification. The *in situ* BBB permeability can be predicted by the *in combo* PAMPA model to a satisfactory degree, and can be used as a lower-cost, high throughput first-pass screening method for BBB passive permeability.

© 2009 Elsevier B.V. All rights reserved.

1. Introduction

Discovery of central nervous system (CNS) drugs is challenging due to the complexity of neurological disorders, the paucity of pre-clinical models with proven human translational value, and the persistent difficulty of delivering drug molecules across the blood–brain barrier (BBB) to achieve optimal CNS exposure. There is an intricate debate taking place in the recent literature regarding how best to interpret the results obtained from *in vitro*, *in situ*, and *in vivo* blood–brain transport methodologies, to identify properties most relevant to successful CNS drug delivery, both in terms of the rate and the extent of penetration (Hammarlund-Udenaes et al., 2008; Martin, 2004; Liu et al., 2005, 2008; Hitchcock, 2008; Jeffrey and Summerfield, 2007; Cecchelli et al., 2007; Maurer et al., 2005; Pardridge, 2007; Reichel, 2009).

The brain-to-plasma distribution ratio has been widely used in drug discovery as an index of brain penetration ($K_p = AUC_{tot,brain}/AUC_{tot,plasma}$, where AUC is the area under the *total* drug concentration–time curve in the corresponding tissue over a dosing interval; also called logBB—see Glossary). However, K_p used in isolation is a misleading parameter since it is generally accepted that it is the *unbound* drug that exerts the physiological effect (Hammarlund-Udenaes et al., 2008; Martin, 2004). Efforts to optimize CNS candidate selections based solely on K_p “may actually lead to unproductive/counterproductive design of drugs that are unnecessarily basic, lipophilic, and have greater degree of nonspecific partitioning into brain tissue” (Maurer et al., 2005). Increasing lipophilicity does not necessarily lead to increased efficacy (Summerfield et al., 2006), and may lead medicinal chemists astray in a chemical space that is hardly druggable due to poor solubility and metabolic instability.

A number of CNS drug discovery groups (Liu et al., 2005, 2008; Jeffrey and Summerfield, 2007; Summerfield et al., 2006) have proposed optimization strategies based on an integrated use of BBB permeability, the effect of efflux transport, and nonspecific plasma and brain tissue binding, to ultimately characterize brain penetration in terms of *in vivo unbound* drug brain distribution: $K_{p,uu} = C_{u,brain}/C_{u,plasma}$, where $C_{u,brain}$ and $C_{u,plasma}$ are the steady-state unbound concentrations in the brain (extracellular fluid)

[☆] Contribution number 18 in the PAMPA—a Drug Absorption *in vitro* Model series from pION. Avdeef, 2005 is part 17 in the series.

* Corresponding author. Tel.: +1 781 935 89 39x22; fax: +1 781 935 89 38.

E-mail address: aavdeef@pion-inc.com (A. Avdeef).

¹ Current address: Amgen Inc., Neurosciences Dept., Thousand Oaks, CA 91320, USA.

and plasma (or blood), respectively (Hammarlund-Udenaes et al., 2008). Ideally, a CNS drug would achieve a $K_{p,uu}$ close to unity within a relatively short time to maximize CNS exposure. In practice, this would also maximize peripheral safety margins by minimizing differences in peak unbound concentrations between brain and plasma. For instance, BBB efflux makes $K_{p,uu} < 1$, requiring higher free plasma concentrations to elicit a CNS effect.

In vivo microdialysis has been the long standing and labor-intensive standard methodology to measure unbound concentrations in living brain (Hammarlund-Udenaes et al., 2008; Fridén et al., 2007; Benveniste and Huttemeier, 1990). A more refined consideration of the *in vivo* ratio, $K_{p,uu}$ (cf., Glossary), draws a distinction between the concentration in the brain homogenate and the brain interstitial fluid (ISF), since the process of homogenization blends the intra- and extracellular brain fluids, which is relevant to compounds with poor cell membrane permeability that may distribute poorly to intracellular compartments. Nevertheless, there is cumulating evidence that suggests measurement of $K_{p,uu}^{in\ vitro}$ can be used to approximate free exposure in a pharmacologically meaningful manner. *In vitro* methods to assess the unbound drug fractions in plasma, $f_{u,plasma}$, and brain tissue homogenates, $f_{u,brain}$, have been extensively investigated (Liu et al., 2005, 2008; Jeffrey and Summerfield, 2007; Maurer et al., 2005; Kalvass and Maurer, 2002; Mahar Doan et al., 2004; Kalvass et al., 2007; Wan et al., 2007; Summerfield et al., 2007).

Many different *in vitro* BBB models have been developed and proposed to measure permeability, some based on human brain endothelial cells (Terasaki et al., 2003; Garberg et al., 2005; Weksler et al., 2005; Abbott, 2007). Despite limited successes, these models generally suffer from a significant loss in transporter function and poor tight junction organization (leakiness) as compared to the *in vivo* BBB. Many drugs companies simply use epithelial cells transfected with P-glycoprotein (MDCK or LLC-PK1) to conduct permeability screening in CNS drug discovery.

Kalvass et al. (2007) provided an integrated approach for assessing CNS steady-state distribution of drugs. They combined the Pgp efflux ratio, ER, with *in vitro*-measured unbound plasma and brain tissue concentrations. A plot of ER vs. $C_{u,plasma}/C_{u,brain}$ is divided into four brain penetration classifications (BPC) using three-fold cutoffs as delineators.

In a similar example of integrative approach to better understand CNS exposure, Liu et al. (2005, 2008) incorporated independent measures of BBB permeability by brain perfusion in their physiologically based pharmacokinetic (PBPK) model, and calculated brain equilibration half-time as $t_{1/2,eq} = \text{const.}/(PS \cdot f_{u,brain})$, where the unbound brain fraction, $f_{u,brain} = C_{u,brain}/C_{tot,brain}$. PS is the product of BBB permeability and the microcapillary specific surface area.

Given the number of compounds to test in early drug discovery, costly and labor-intensive *in vivo* measurements of CNS pharmacokinetic properties are impractical, and *in vitro* BBB models rely on relatively time-consuming cell culture. Useful *in silico* predictions of *in vivo* BBB transport properties could substitute for direct measurements in initial screening. *In silico* methods to predict K_p exist (Bendels et al., 2008; Zhang et al., 2008; Kortagere et al., 2008), but have not been applied to $K_{p,uu}$. The prediction of $PS_{passive}$ has been the subject of a number of studies (Clark, 2003; Abraham, 2004; Lanevskij et al., 2008; Di et al., 2008). *In silico* attempts have been made to estimate the influence of Pgp on *in vitro* substrate transport (Didziapetris et al., 2003; Garg and Verma, 2006).

The most reliable published PS data come from rodent *in situ* brain perfusion studies (Takasato et al., 1984; Gratton et al., 1997; Wu et al., 1998; Murakami et al., 2000; Bourasset et al., 2003; Cisternino et al., 2003a,b, 2004a,b; Youdim et al., 2004; Dagenais, 2000; Dagenais et al., 2000, 2001, 2002, 2004, 2005;

Cisternino et al., 2004a,b; Liu et al., 2005; Parepally et al., 2006; Bihorel et al., 2007; Obradovic et al., 2007). The modified Takasato method (Takasato et al., 1984) has been adapted to the mouse by Dagenais and Rousselle (Dagenais et al., 2000), and applied to study BBB efflux using various knockout mouse models. This technique requires special surgical skills, is labor and animal intensive, and time consuming. Unless radiolabeled compounds are used, significant bioanalytical resources are required (e.g., liquid chromatography-mass spectrometry). Rodent brain perfusion studies are not performed routinely in the pharmaceutical industry.

As a cost-effective high-throughput alternative to *in vitro* and *in situ* methods to estimate BBB permeability, PAMPA (parallel artificial membrane permeability assay) could be used to assess $PS_{passive}$ (Kansy et al., 1998; Avdeef, 2003, 2005; Di et al., 2003, 2008; Bermejo et al., 2004; Avdeef et al., 2004, 2005; Youdim et al., 2003; Ruell et al., 2004). PAMPA membranes are based on a mixture of phospholipids deposited into lipophilic microfilters, and contain net-negative lipid charge, mimicking some of the properties of endothelial cell membranes. Di et al. (2003) adapted porcine brain lipid extract dissolved in *n*-dodecane (2%, w/v) as their PAMPA membrane barrier and demonstrated that molecules can be successfully binned into CNS+ and CNS- classes. The early attempts to establish a numerical relationship between PAMPA and Caco-2 cellular assays have shown considerable promise, with high linear correlations reported (Bermejo et al., 2004). An *in combo* PAMPA method (hybrid “combination” of *in silico* and *in vitro* methods) has been described, where it was possible to separate some active and passive components of cellular permeability (Avdeef et al., 2005).

In this study, we report 38 new *in situ* PS measurements performed on 19 compounds in wild-type (WT) and Pgp-deficient [*mdr1a*(-/-)] CF-1 mice (so called mutants equivalent in phenotype to the corresponding “knockout” model). One aim of the study was to quantify the influence of Pgp on PS values by comparing the mouse genotypes. The second aim was to use $PS_{passive}$ values from the Pgp deficient data to train the *in combo* PAMPA procedure, followed by enhancement and validation based on additional published rodent values. We were interested in developing a practical, cost-effective, and rapid quantitative *in combo* assay which could be used in early screening for passive BBB permeability, and which could over time assist medicinal chemists with structure modification to improve a key determinant of CNS exposure for test compounds downstream in the discovery process, as part of an integrated BBB penetration model, incorporating $PS_{passive}$ along with possibly ER, $f_{u,brain}$, and $f_{u,plasma}$. Finally we explored the implicit contribution of passive BBB permeability in the brain penetration classification (BPC), which has not been discussed in the published literature.

2. Materials and methods

2.1. Drugs and chemicals

The unlabeled chemicals used in this study (training set) were purchased from Sigma-Aldrich/RBI (St. Louis, MO, USA) and Tocris Bioscience (Ellisville, MO, USA), and used as received, except that analytical-grade amitriptyline and indinavir (Merck), astemizole, domperidone and galanthamine (Janssen-Ortho), clozapine (Novartis), gabapentin and sertraline (Pfizer), ritonavir (Abbott), saquinavir (Roche), and terfenadine (Aventis), were kindly provided by their manufacturer. PAMPA lipid (lecithin mixture) was obtained from pION (PN 110669), and was stored at -20°C when not used. The pH of the assayed donor solutions was adjusted with a universal buffer (pION, PN 100621). A buffer solution at pH 7.4 containing a chemical scavenger to simulate tissue binding and

maintain sink conditions (pION ASB-7.4 buffer, PN 110139) was used as the receiver solution.

2.2. Animals

Adult male CF-1 mice (wild-type and *mdr1a*(-/-), 30–40 g, 6–8 weeks old) were obtained from Charles River Laboratories (Wilmington, MA, USA). Animals were housed in a room with a controlled environment ($22 \pm 3^\circ\text{C}$; $55 \pm 10\%$ relative humidity) and maintained under a 12-h dark:light cycle (light from 6 a.m. to 6 p.m.). Animals had access to food and tap water *ad libitum*. All animal experiments were evaluated and approved by the Institutional Committee for Good Animal Practices (UQAM, Montréal, Québec, Canada).

2.3. Mouse brain perfusion technique

2.3.1. Surgical procedure and transport studies

The *in situ* mouse brain perfusion has been described in detail elsewhere (Dagenais, 2000; Dagenais et al., 2000). Briefly, mice were anesthetized with intraperitoneal ketamine/xylazine (140/8 mg/kg). The right hemisphere was perfused through the right common and internal carotid arteries following ligation of the external branch. The cardiac ventricles were severed immediately before brain perfusion (Krebs-bicarbonate buffer gassed to pH 7.4 with 95% O_2 and 5% CO_2 at 37°C) at 2.5 mL/min via a syringe pump. Test compounds were spiked in perfusate at a targeted concentration of $1 \mu\text{M}$ from a DMSO or dilute acetic acid stock solution (400-fold dilution). The perfusions were terminated by decapitation. Single time point experiments were performed (1, 2 or 3 min) based on the molecular properties of the compounds and their expected permeability category (low, intermediate, high). Previous studies were used to gauge the length of perfusion most likely to be within the linear portion of the uptake curve. The brain was removed from the skull and dissected on ice to isolate the right hemisphere. At this point, a sample of perfusion fluid was collected at the tip of the catheter by activation of the infusion pump. Samples were frozen in liquid nitrogen and maintained at -80°C until analysis by LC/MS or LC/MS/MS.

2.3.2. Sample preparation and bioanalysis

The generic sample preparation and bioanalysis procedures have been reported in detail elsewhere (Dagenais et al., 2002, 2004). As appropriate, samples of perfusion fluid were acidified with 1% (v/v) glacial acetic acid, and diluted with the mobile phase used at the start of gradient elution without further preparation. Brain samples (ca. 150 mg) were homogenized in 4 volumes of aqueous buffer, followed by protein precipitation with 2 volumes of ice-cold acetonitrile. Following centrifugation, the supernatant was either injected directly onto the HPLC system, or evaporated and reconstituted in 40% acetonitrile/60% water with 0.1% formic acid. All *in vivo* samples were quantified by LC/MS or LC/MS/MS using an Agilent 1100 LC/MSD system (Agilent Technologies, Wilmington, DE), or a PE-Sciex API-3000 MS/MS system (Applied Biosystems, Foster City, CA) fitted with a Shimadzu LC-10 HPLC system (Shimadzu Scientific Systems, Columbia, MD) and a CTC-Pal autosampler (Leap Technologies, Carrboro, NC). Gradient elution (1–2 mL/min) using admixtures of 0.1% formic acid or 25 mM acetate, and acetonitrile or methanol, was applied to high performance analytical columns (Agilent Zorbax C-18, YMC NH2 or Agilent Zorbax Extend C-18, all 4.6 mm \times 50 mm). Parent ion monitoring (i.e., selective ion monitoring, MS) or multiple reaction monitoring (MS/MS) were used for mass spectrometric detection. Diclofenac was used as the internal standard. Typical run times

were between 2 and 8 min per sample. Calibration curves were fit using linear or quadratic relationships with standard software from the instruments' manufacturer. A deviation of 20% or less from the predicted curve was considered acceptable for points on the calibration curve. Samples were re-assayed after appropriate dilution if the concentration could not accurately be interpolated or extrapolated.

2.3.3. Calculation of the *in situ* BBB permeability

Initial uptake data from brain perfusion experiments can be assimilated to a pharmacokinetic tissue uptake clearance (Dagenais, 2000; Dagenais et al., 2000), but traditionally have been referred to as K_{in} values, which can be estimated from single time point experiments using the following relationship (Dagenais, 2000; Dagenais et al., 2000), $K_{in} = (X_{br}/T)/C_{pf}$, where X_{br} is parenchymal brain concentration (mol/kg units) of the tracer, C_{pf} is the perfusion fluid (analogous to arterial) concentration (mol/L) of the test compound collected at the tip of the infusion catheter, T is the perfusion time (min), and K_{in} is the initial rate of brain uptake. Parenchymal brain concentration is obtained by subtracting from the total concentration, the contribution from the vascular volume, $X_{br} = X_{total} - V_{vasc}C_{pf}$. A vascular volume of 1 mL/100 g was used to correct total brain concentrations.

Using the Crone–Renkin equation, the rate constant is defined as $K_{in} = F_{pf}(1 - e^{-PS/F_{pf}})$, where F_{pf} is the regional cerebral flow of perfusion fluid, and PS is the capillary permeability-surface area product. Usually, diazepam is used as a flow marker to determine F_{pf} , since its uptake clearance is expected to be maximal (Dagenais, 2000; Dagenais et al., 2000). However, in the training set used in this study, three compounds (amitriptyline, buspirone, chlorpromazine) had brain uptake clearances that were greater than that of diazepam (255 mL/100 g/min in the mouse; Dagenais, 2000; Dagenais et al., 2000). Since the results tend to be more variable and sensitive to changes in experimental conditions under a flow-limited situation, the regional cerebral flow, F_{pf} , was taken to be 430 mL/100 g/min for the purpose of the training set conversions. This value was selected so that all of the measured K_{in} may be converted to PS values. This choice did not alter the ranking of the PS values, as considered below.

In order to apply the Abraham descriptors, the PS value were temporarily converted to the intrinsic scale (Avdeef et al., 2005), according to the equation $P_o^{BBB} = (PS/S)(1 + 10^{\pm(pH-pK_a)})$, with the '+' used for acids, and the '-' sign used for bases, and where S = brain capillary surface area, assumed to be $100 \text{ cm}^2/\text{g}$ (Ohno et al., 1978).

2.3.4. Pgp effect

In addition to Pgp deficient (*mdr1a*(-/-)) data, wild-type mouse uptake clearance data were measured in this study. The results from Pgp-deficient mice were expected to result in a better estimate of passive permeability. The Pgp effect is defined by the ratio of the Pgp-deficient uptake clearance to that of wild-type up uptake clearance.

3. PAMPA method

3.1. Data collection

The PAMPA Evo instrument from pION INC (Woburn, MA, USA) was used in this study. The 96-well microtitre plate "sandwich" (pION, PN 110212, preloaded with magnetic stirrers) filters were coated with a 20% (w/v) alkane solution of a lecithin mixture containing an excess of negatively charged constituents (pION, PN 110669). Sample concentrations in the buffer solutions for the compounds with low-UV absorption were about $500 \mu\text{M}$ (e.g.,

gabapentin, DPDPE, meperidine). However, for most of the compounds, UV sensitivity was good, and the typical concentrations were about 50 μM . DMSO-free stock solutions were prepared for some of the compounds (buspirone, colchicine, quinidine, tolbutamide, U69593, fentanyl, sertraline, ritonavir, astemizole, clozapine, deltorphin II, DPDPE, gabapentin, galanthamine, indinavir), to improve on UV sensitivity in the 210–240 nm part of the spectrum. The donor solutions were varied in pH (NaOH-treated universal buffer), while the receiver solutions had the same pH 7.4. This was necessary in order to correct the effective permeability values for ionization and aqueous boundary layer (ABL) effects (Avdeef et al., 2004, 2005). The $\text{pK}_a^{\text{flux}}$ -centered (see below) gradient pH values were selected by the *pOD* procedure (Ruell et al., 2003). The receiver solutions contained a surfactant mixture (“lipophilic sink”) to mimic tissue binding (Avdeef, 2003). Vigorous stirring was employed in the assay, with stirring speed set to produce an ABL thickness $<50 \mu\text{m}$, to minimize the ABL contribution to the measured permeability. The PAMPA sandwich was assembled and allowed to incubate for 30 min for highly permeable molecules (e.g., amitriptyline, chlorpromazine, loperamide, sertraline, probenecid and verapamil), and 15 h for poorly permeable molecules (e.g., galanthamine, DPDPE, deltorphin II, indinavir), in a controlled-environment chamber (*pION* PN 110205) with a built-in magnetic stirring mechanism. Both the donor and receiver wells were assayed for the amount of material present, by comparison with the UV spectrum (210–500 nm) obtained from a reference standard. Permeability values were corrected for membrane retention (Avdeef, 2003).

3.2. Correcting PAMPA permeability for the ABL and charge effects by the $\text{pK}_a^{\text{flux}}$ method

In brain endothelial microcapillaries, the ABL thickness is likely to be $<1 \mu\text{m}$ (given that the radius of the human microcapillaries is about $3 \mu\text{m}$), whereas in unstirred PAMPA, the ABL thickness can be as high as $4000 \mu\text{m}$ (Avdeef et al., 2004). By taking PAMPA (stirred or unstirred) data over a range of pH, it is possible to correct for the effect of the ABL, by applying the $\text{pK}_a^{\text{flux}}$ method (Avdeef, 2003; Avdeef et al., 2004, 2005; Ruell et al., 2003), briefly described below.

In the analysis of PAMPA data, four types of permeability values are considered: (a) the effective permeability coefficient, P_e (which is directly determined); (b) the aqueous boundary layer permeability, P_{ABL} , based on the resistance of the water layer adjacent the membrane; (c) the membrane permeability, P_m (which depends on pH with ionizable molecules); and (d) the intrinsic permeability, P_o , which is the permeability of the uncharged species (the maximum possible value of P_m at the pH where an ionizable molecule is uncharged). ABL-limited transport is often observed for lipophilic molecules, when $P_o \gg P_{\text{ABL}}$. The basic equation describing permeability is (Avdeef et al., 2005)

$$\log P_e = \log P_e^{\text{max}} - \log(10^{\pm(\text{pH}-\text{pK}_a^{\text{flux}})} + 1) \quad (1)$$

which is valid provided that $P_o > 10 P_{\text{ABL}}$ (lipophilic molecules). The maximum possible effective (measured) permeability, P_e^{max} , is defined as $\log P_e^{\text{max}} = \log P_{\text{ABL}} - \log(1 + P_{\text{ABL}}/P_o)$. When $P_o \gg P_{\text{ABL}}$ (highly permeable molecules), $P_e^{\text{max}} \approx P_{\text{ABL}}$. The “flux” ionization constant, $\text{pK}_a^{\text{flux}}$, refers to the pH value where the resistance to transport across a permeation barrier is 50% due to the ABL and 50% due to the membrane (Avdeef, 2003).

4. *In silico* model building software and the *in combo* strategy

4.1. PS training and test set selection criteria

Our core computational object was to model $\text{PS}_{\text{passive}}$ values. From a survey of the published literature, 507 PS values were identified, based on *in vivo* intravenous injection (i.v.), bolus carotid artery injection (BUI), and *in situ* brain perfusion methods, for rats, mice, guinea pigs, rabbits, dogs, and cats. It was decided to focus only on rat ($n = 335$, 66%) and mouse ($n = 131$, 26%) data, accounting for about 92% of the collected values.

It is hypothesized here that mouse and rat data are comparable for the purposes of our prediction study. This may be reasonable, as suggested by Murakami et al. (2000). For their reported rat and mouse permeability values (21 compounds), the linear regression of rat vs. mouse logarithm of the intrinsic (defined below) permeability coefficients yielded the intercept = 0.21 ± 0.24 and slope = 1.01 ± 0.05 .

Since plasma protein binding lowers values of PS (in comparison to protein-free perfusate experiments), i.v. data were not used for lipophilic compounds. Compounds that had reported saturable transport were also excluded. Since we were interested to select *in situ* data as free of efflux effects as practical, we chose our training set PS values from studies which used some sort of transport inhibition (e.g., Pgp-KO, cyclosporine A, PSC833, GF120918, self-inhibition by using high concentrations). Also, simple amino acids and dipeptides were excluded, except for those with reported non-saturable K_d values. In our own data, the L-isomer of p-F-phenylalanine was excluded from the training set, since comparison with the D-isomer clearly indicated that its transport was facilitated. As an added pruning, several compounds were excluded from the training set on the suspicion that carrier-mediated transport was possible, by comparisons of structures to known transport-mediated molecules. Out of the starting set of 507 PS values, a total of 182 “passive” rodent values were selected in our study, including the *in situ* measurements reported here.

The *in combo* PAMPA model was trained with a set of 80 compounds: 31 bases, 11 acids, 15 ampholytes, and 23 neutral molecules (encompassing 130 different measured PS values). In addition to the 130-PS training set, an additional 52 molecules (Summerfield et al., 2007; Gratton et al., 1997; Obradovic et al., 2007) were taken to serve as the test set. Table 1 contains physical properties and the Abraham (2004) descriptors of the training and test set molecules.

4.2. Linear free energy relations (LFER) descriptors “boosting” PAMPA measured values

Abraham’s linear free energy relations (LFER) applied to a BBB permeability model may be stated as (Abraham, 2004)

$$\log P_o^{\text{BBB}}(\text{LFER}) = c_0 + c_1R + c_2\pi + c_3\alpha + c_4\beta + c_5V_x \quad (2)$$

where c_0, \dots, c_5 are the multiple linear regression (MLR) coefficients, and where R ($\text{dm}^3 \text{mol}^{-1}/10$; also called E) is the excess molar refraction, which models dispersion force interaction arising from pi- and n-electrons of the solute, π (also called S) is the solute polarity/polarizability due to solute–solvent interactions between bond dipoles and induced dipoles, α (also called A) is the solute H-bond acidity, β (also called B) is the solute H-bond basicity, and V_x is the McGowan molar volume ($\text{dm}^3 \text{mol}^{-1}/100$) of the solute.

Eq. (2) uses intrinsic BBB permeability values, P_o^{BBB} , rather than PS values. This is because the Abraham molecular descriptors have been developed for uncharged species, and so it was decided to convert all permeability values (PS and PAMPA) to intrinsic values, P_o^{BBB} and P_o^{PAMPA} , in order to develop the computational model. This

Table 1
Physical properties, Abraham descriptors, and PAMPA^a.

Compound	MW	log <i>P</i> _{oct}	log <i>D</i> _{oct}	p <i>K</i> _a	<i>f</i>	(<i>Q</i>)	α (<i>A</i>)	β (<i>B</i>)	π (<i>S</i>)	<i>R</i> (<i>E</i>)	<i>V</i> _x	log <i>P</i> ₀ ^{PAMPA}	SD	Ref	
<i>Training set</i>															
1-Aminocyclohexanecarboxylic acid	143	-1.6	-1.6	9.1	2.1	1.00	(±)	0.78	0.93	0.98	0.56	1.16	-7.05	b	-
3-Hydroxykynurenine	224	-2.6	-2.6	9.9	2.3	0.95	(±)	1.31	1.71	2.19	1.70	1.63	-8.65	b	-
Amitriptyline	277	4.9	3.5	9.49		0.96	(+)	0.00	0.77	1.31	1.71	2.40	1.30	0.04	d
Antipyrine	188	0.8	0.8			1.00	(0)	0.00	1.28	1.75	1.42	1.48	-5.69	0.03	e
Astemizole	459	5.5	3.9	8.60	5.84	0.94	(+)	0.13	1.64	2.70	3.10	3.56	1.00	0.10	f
Bremazocine	315	3.4	3.2	10.3	8.5	0.66	(0)	0.73	1.35	1.28	1.82	2.58	-1.49	0.07	c
Buspirone	386	2.7	2.2	7.60		0.67	(+)	0.00	2.16	2.18	2.22	3.03	-2.88	0.08	c
Carbamazepine	236	2.5	2.5			1.00	(0)	0.39	0.92	2.06	2.12	1.81	-3.73	0.17	c
Cetirizine	389	2.6	-0.4	7.9	3.8	0.76	(±)	0.57	1.76	2.24	2.05	2.94	-3.24	b	-
Chlorpromazine	319	5.4	3.7	9.24		0.98	(+)	0.00	0.99	1.83	2.26	2.41	1.62	0.08	e,g
Cimetidine	252	0.7	0.6	6.93		0.80	(0)	0.74	1.86	1.87	1.66	1.96	-6.20	0.08	h
Clozapine	327	3.1	2.6	7.90	4.40	0.71	(+)	0.18	1.44	1.82	2.46	2.43	-0.39	0.09	c
Colchicine	399	1.2	1.2			1.00	(0)	0.26	2.08	3.32	2.17	2.99	-5.40	0.01	c
Creatinine	113	-1.1	-1.1	9.2	4.8	1.00	(0)	0.39	1.31	1.04	1.04	0.84	-7.52	0.10	c
Deltorphin II	783	-0.8	-3.5	10.10	4.27	0.56	(-)	3.30	5.53	8.18	4.06	6.03	-6.37	0.02	c
Diazepam	285	2.8	2.8	3.40		1.00	(0)	0.00	1.04	1.72	2.11	2.07	-2.44	0.29	c
Digoxin	781	1.4	1.4			1.00	(0)	1.58	4.32	4.46	3.67	5.75	-5.78	0.08	c
Diltiazem	415	3.1	2.4	8.02		0.80	(+)	0.00	2.12	2.55	2.42	3.14	-1.33	0.01	h
Diphenhydramine	255	3.5	2.2	9.10		0.95	(+)	0.00	0.95	1.43	1.36	2.19	-0.71	0.08	d
Domperidone	426	4.2	3.9	8.10		0.51	(+)	0.72	1.83	3.13	3.11	3.06	-2.78	0.11	c
Doxepin	279	4.1	2.7	9.5		0.96	(+)	0.00	0.98	1.46	1.75	2.32	0.44	0.08	g
DPDPE	646	-0.9	-3.7	10.1	3.5	0.55	(-)	2.30	4.04	5.81	3.87	4.77	-7.31	0.19	c
Estradiol	272	3.1	3.1	10.4		1.00	(0)	0.81	0.95	2.30	1.85	2.20	-3.08	0.02	c
Etoposide	589	0.6	0.6	10.0		1.00	(0)	0.60	3.23	4.11	3.38	3.90	-5.22	0.01	c
Fentanyl	336	4.0	3.4	8.10		0.76	(+)	0.00	1.33	2.18	1.86	2.84	-0.95	0.07	c
Fexofenadine	502	4.8	2.2	7.84	4.3	1.00	(±)	1.20	2.12	2.48	2.72	4.09	-5.17	0.03	c
Flurbiprofen	244	3.9	0.7	4.18		1.00	(-)	0.57	0.58	1.51	1.50	1.84	-1.78	0.01	g
Gabapentin	185	0.2	0.2	10.6	3.8	1.00	(±)	0.78	0.96	1.02	0.59	1.58	-3.36	0.31	c
Galanthamine	287	1.2	-0.1	8.6		0.96	(+)	0.31	1.45	1.92	1.89	2.17	-3.15	0.04	c
Glibenclamide	494	4.4	2.1	5.90		0.97	(-)	0.85	2.01	3.84	2.64	3.56	-2.54	0.08	f
Grepafloxacin	359	0.2	-2.1	8.5	6.0	0.91	(±)	0.73	1.88	2.43	2.23	2.59	-4.87	b	-
Haloperidol	376	3.7	2.7	8.65		0.88	(+)	0.31	1.45	2.08	2.00	2.80	0.05	0.05	d
HSR-903	386	-0.1	-2.2	10.6	6.1	0.86	(±)	0.98	2.24	2.78	2.80	2.72	-5.46	b	-
Hydroxyzine	375	3.2	3.1	7.5		0.84	(0)	0.23	1.80	2.01	2.12	2.92	-1.50	0.12	c
Ibuprofen	206	3.4	0.4	4.59		1.00	(-)	0.57	0.51	1.01	0.78	1.78	-2.11	0.09	g,i
Imatinib	494	3.7	3.3	7.6	4.7	0.61	(+)	0.54	2.63	3.64	3.83	3.85	-1.40	0.30	c
Indinavir	614	3.3	3.3	6.2		0.91	(0)	0.98	3.59	4.27	3.63	4.90	-3.57	0.07	c
Indomethacin	358	4.4	1.6	4.57		1.00	(-)	0.57	1.24	2.49	2.44	2.53	-1.65	0.25	e,g
Lidocaine	234	2.2	1.6	7.95		0.76	(+)	0.26	1.17	1.50	1.10	2.06	-1.42	0.15	d
L-Kynurenine	208	-2.2	-2.2	9.9	2.3	0.98	(±)	0.96	1.60	2.06	1.50	1.57	-7.82	b	-
L-Leucine	131	-1.8	-1.8	9.1	2.1	1.00	(±)	0.78	0.97	0.92	0.39	1.13	-7.25	b	-
Loperamide	477	4.7	3.8	8.5		0.88	(+)	0.31	1.88	2.90	2.76	3.77	0.15	0.06	c
L-Phenylalanine	165	-1.4	-1.4	9.23	2.20	0.98	(±)	0.78	1.02	1.39	0.95	1.31	-5.36	0.06	c
L-Valine	117	-2.2	-2.2	9.1	2.1	1.00	(±)	0.78	0.97	0.92	0.39	0.99	-7.54	b	-
M6G	461	-1.6	-4.2	8.22	2.77	0.78	(±)	1.64	2.84	2.96	3.10	3.11	-7.66	b	-
Maprotiline	277	5.1	2.2	10.4		1.00	(+)	0.13	0.68	1.27	1.76	2.33	1.99	0.06	g
Melphalin	305	-0.3	-0.3	9.1	2.1	0.98	(±)	0.78	1.37	1.90	1.43	2.22	-5.87	b	-
Meperidine	247	2.6	1.3	8.58		0.94	(+)	0.00	0.97	1.26	0.99	2.05	0.79	0.20	c
Methadone	309	3.9	2.6	8.99		0.95	(+)	0.00	1.09	1.72	1.51	2.71	0.08	0.03	c
Morphine	285	0.9	0.3	9.46	8.13	0.76	(+)	0.50	1.47	1.59	2.23	2.06	-3.59	0.12	g
Naltrindole	414	3.3	2.3	10.0	8.3	0.89	(+)	1.04	1.92	3.16	3.53	2.98	-0.94	0.10	c
Naringenin	272	2.5	2.5	10.4	8.9	0.97	(0)	1.30	1.14	2.19	2.23	1.89	-3.71	0.06	c
Perphenazine	404	4.2	3.6	7.9		0.75	(+)	0.23	1.84	2.33	2.87	3.02	0.81	0.14	c
p-F-Phe(D)	183	-1.5	-1.5	9.2	2.2	0.98	(±)	0.78	1.02	1.36	0.87	1.33	-6.73	0.09	c

Table 1 (Continued)

Compound	MW	log P_{oct}	log D_{oct}	pK _a	f	(Q)	α (A)	β (B)	π (S)	R (E)	V_x	log P_0^{PAMPA}	SD	Ref
Phenytoin	252	2.3	2.3	8.36	0.89	(0)	0.44	1.14	2.04	1.94	1.87	-4.32	0.01	g
Prazosin	383	0.9	0.8	7.14	0.80	(0)	0.23	2.17	3.59	2.94	2.74	-2.58	0.03	g
Probenecid	285	2.9	-0.7	3.16	1.00	(-)	0.57	1.29	1.92	1.25	2.16	-1.83	0.20	g
Propranolol	259	3.0	0.9	9.53	0.99	(+)	0.29	1.36	1.44	1.76	2.15	0.43	0.38	g,h
Quercetin	302	1.9	1.3	9.40	6.90	(-)	1.88	1.63	2.64	2.68	1.96	-4.77	0.22	c
Quetiapine	384	2.4	2.4	7.30	2.27	(0)	0.23	2.01	1.93	2.72	2.91	-1.85	0.02	c
Quinidine	324	2.9	1.6	8.55	4.09	(+)	0.23	1.81	1.71	2.40	2.55	-1.56	0.07	g
Quinine	324	2.9	1.6	8.55	4.09	(+)	0.23	1.81	1.71	2.40	2.55	-1.05	0.08	i
Risperidone	410	2.9	2.1	8.2	0.86	(+)	0.00	1.70	2.23	2.59	3.04	-2.01	0.07	c
Ritonavir	693	4.9	4.9	4.1	1.00	(0)	0.88	3.11	5.05	3.69	5.27	-1.68	0.18	c
Salicylic acid	138	2.4	-1.6	3.02	1.00	(-)	0.70	0.40	1.10	0.91	0.99	-2.64	0.13	i
Saquinavir	671	4.0	4.0	6.8	0.86	(0)	1.46	3.89	5.55	4.09	5.30	-3.69	0.07	c
Sertraline	306	4.9	2.8	9.5	0.99	(+)	0.13	0.67	1.44	1.83	2.26	2.10	0.09	c
SNC121	452	4.5	3.6	7.7	4.1	(+)	0.00	2.11	2.47	2.12	3.84	-1.24	0.09	c
Sumatriptan	295	1.3	0.0	9.64	8.93	(+)	0.68	1.61	2.05	1.90	2.27	-4.18	0.09	j
Terfenadine	472	5.8	3.5	9.86	1.00	(+)	0.63	1.80	2.04	2.55	4.01	2.63	0.17	g,k
Testosterone	288	3.1	3.1	3.1	1.00	(0)	0.31	1.01	2.27	1.55	2.38	-2.83	0.01	c
Theophylline	180	0.1	0.1	8.70	0.95	(0)	0.35	1.29	1.99	1.46	1.22	-5.99	0.02	d
Thioridazine	371	6.2	4.2	8.82	0.99	(+)	0.00	1.13	1.93	2.70	2.90	1.81	0.17	c
Tiagabine	376	5.8	3.3	9.0	3.7	(±)	0.57	1.02	1.60	1.77	2.89	0.32	b	-
Tolbutamide	270	2.3	0.1	5.20	0.99	(-)	0.59	1.15	2.21	1.33	2.06	-3.70	0.02	c
U69593	357	3.6	2.4	9.3	0.94	(+)	0.00	1.49	2.07	1.73	2.92	0.37	0.18	c
Verapamil	455	4.3	2.9	9.07	0.96	(+)	0.00	1.89	3.00	1.76	3.79	0.26	0.12	g,h
Vinblastine	811	4.1	3.8	7.4	6.0	(0)	0.54	4.01	3.72	4.46	6.07	-0.42	0.05	c
Vincristine	825	3.1	2.8	7.4	5.4	(0)	0.54	4.25	4.30	4.59	6.08	-2.72	0.06	c
Warfarin	308	2.9	-0.2	4.97	1.00	(-)	0.31	1.23	2.28	1.98	2.31	-2.59	0.06	g
Zidovudine	267	0.0	0.0		0.93	(0)	0.47	1.70	1.77	1.62	1.82	-5.79	0.17	c
<i>Test set</i>														
Amantadine	151	2.4	-0.4	10.5	1.00	(+)	0.21	0.64	0.68	0.84	1.29	-1.12	b	-
Amoxapine	314	2.1	1.8	7.6	0.54	(+)	0.16	1.43	1.68	2.25	2.25	-1.89	b	-
Atomoxetine	255	3.6	1.5	10.3	0.99	(+)	0.13	0.90	1.36	1.37	2.19	-0.13	b	-
AZ 11003	503	5.0	3.1	8.10	0.99	(+)	0.41	1.95	2.83	1.84	3.92	0.58	b	-
AZ 12002	393	2.7	-0.4	3.20	1.00	(-)	0.57	1.43	2.14	2.28	2.40	-3.14	b	-
AZ 13007	163	2.4	-0.4	10.10	1.00	(+)	0.21	0.73	0.75	1.11	1.32	-1.12	b	-
AZ 22001	216	-0.2	-4.3	5.30	1.00	(-)	0.23	1.17	2.50	1.21	1.41	-4.91	b	-
AZ 26006	637	5.4	3.4	8.91	0.99	(+)	0.43	3.18	3.74	2.79	4.80	0.96	b	-
AZ 95005	251	1.5	1.5		1.00	(0)	0.48	1.33	1.87	1.18	2.08	-4.40	b	-
Brompheniramine	319	3.2	1.5	9.2	0.98	(+)	0.00	1.02	1.57	1.70	2.26	-0.37	b	-
Bupropion	240	2.9	1.6	8.8	0.95	(+)	0.13	0.94	1.32	1.07	1.94	-0.94	b	-
Chlorpheniramine	275	3.1	1.3	9.2	0.98	(+)	0.00	1.02	1.49	1.52	2.21	-0.51	b	-
Citalopram	324	3.8	1.9	9.4	0.99	(+)	0.00	1.08	1.87	1.66	2.53	0.16	b	-
Clemastine	344	5.6	3.4	9.6	1.00	(+)	0.00	0.97	1.55	1.70	2.76	1.82	b	-
Donepezil	379	3.9	2.5	9.2	0.96	(+)	0.00	1.50	2.49	2.12	3.03	0.08	b	-
Ergotamine	582	1.7	1.6	6.9	0.81	(0)	0.79	3.69	4.60	4.56	4.21	-4.71	b	-
Erythritol	122	-2.2	-2.2		1.00	(0)	1.08	1.20	1.23	0.82	0.91	-8.50	b	-
Ethanol	46	-0.2	-0.2		1.00	(0)	0.31	0.31	0.45	0.21	0.45	-5.68	b	-
Ethosuximide	141	0.4	0.4	9.3	0.99	(0)	0.34	0.93	0.94	0.74	1.12	-5.23	b	-
Ethylene glycol	62	-1.3	-1.3		1.00	(0)	0.54	0.58	0.71	0.41	0.51	-6.91	b	-
Fluoxetine	309	4.2	2.0	9.6	0.99	(+)	0.13	0.78	1.19	1.01	2.24	0.35	b	-
Fluphenazine	438	4.4	3.8	7.9	0.75	(+)	0.23	1.80	2.00	2.40	3.09	0.05	b	-
Isocarboxazid	231	1.7	1.7	2.8	1.00	(0)	0.39	1.38	2.16	1.61	1.74	-4.18	b	-
Isopropanol	60	0.3	0.3		1.00	(0)	0.31	0.34	0.43	0.22	0.59	-5.25	b	-
Lamotrigine	256	2.4	2.4	5.5	1.00	(0)	0.45	0.93	2.13	2.40	1.65	-3.62	b	-
Loratidine	383	5.0	5.0	5.0	1.00	(0)	0.00	1.14	2.09	2.19	2.87	-0.69	b	-

Loxapine	328	2.7	2.6	6.7	0.86	(0)	0.00	1.49	1.67	2.30	2.39	-2.70	b
Mannitol	182	-3.2	-3.2		1.00	(0)	1.62	1.81	1.75	1.23	1.31	-10.09	b
Meprobamate	218	1.0	1.0		1.00	(0)	0.89	1.12	1.62	0.71	1.73	-5.43	b
Mesoridazine	387	4.5	2.5	9.4	0.99	(+)	0.00	1.69	2.97	2.87	2.96	0.73	b
Metoclopramide	300	2.5	0.7	9.2	0.98	(+)	0.50	1.63	2.31	1.50	2.34	-1.75	b
Midazolam	326	3.0	3.0	6.4	0.96	(0)	0.00	0.80	1.76	2.41	2.26	-2.45	b
Mirtazapine	265	3.1	2.8	7.5	0.55	(0)	0.00	1.22	1.67	2.08	2.11	-2.32	b
Olanzapine	312	2.7	2.2	7.8	0.72	(+)	0.13	1.45	1.59	2.30	2.37	-1.30	b
Pemoline	176	0.2	0.2	1.3	1.00	(0)	0.21	1.22	1.45	1.48	1.26	-5.21	b
Pergolide	314	5.1	4.3	8.7	0.86	(+)	0.31	1.01	1.48	2.22	2.54	0.61	b
Phenelzine	136	1.1	0.5	7.9	0.76	(+)	0.34	0.99	1.02	0.98	1.20	-3.00	b
Pyrilamine	285	3.1	1.6	8.8	0.96	(+)	0.00	1.45	1.73	1.66	2.39	-0.61	b
Rizatriptan	269	2.4	1.1	8.7	0.95	(+)	0.31	1.28	2.05	2.21	2.14	-1.63	b
Selegiline	187	2.9	2.6	7.3	0.56	(0)	0.09	0.71	1.00	1.00	1.72	-2.64	b
Sucrose	342	-3.4	-3.4		1.00	(0)	2.01	3.43	2.63	2.32	2.23	-10.86	b
Tacrine	198	2.8	0.3	9.9	1.00	(+)	0.23	0.76	1.52	1.88	1.60	-0.91	b
Temazepam	301	2.1	2.1	1.5	1.00	(0)	0.17	1.34	1.76	2.24	2.13	-3.47	b
Thiothixene	444	4.1	3.3	8.1	0.83	(+)	0.00	2.19	2.59	2.94	3.36	0.10	b
Thiourea	76	-1.0	-1.0		1.00	(0)	0.42	0.82	0.97	1.07	0.57	-6.53	b
Thymine	126	-0.7	-0.7		1.00	(0)	0.44	0.90	1.41	0.88	0.89	-6.27	b
Trazodone	372	3.5	3.4	7.0	0.81	(0)	0.00	1.92	2.47	2.64	2.73	-2.01	b
Trifluoperazine	408	5.1	4.3	10.0	0.85	(+)	0.00	1.42	1.79	2.17	2.89	1.02	b
Urea	60	-1.6	-1.6		1.00	(0)	0.72	0.69	1.17	0.63	0.46	-7.43	b
Venlafaxine	277	3.3	2.4	8.7	0.90	(+)	0.31	1.16	1.23	1.20	2.37	-0.91	b
Zaleplon	305	1.8	1.8	1.6	1.00	(0)	0.00	1.42	2.60	2.36	2.31	-3.52	b
Ziprasidone	413	4.6	4.3	7.7	0.52	(0)	0.48	1.65	2.67	3.38	2.92	-1.65	b

^aThe octanol–water partition coefficients, $\log P_{\text{oct}}$, the octanol–water distribution coefficients at pH 7.4, $\log D_{\text{oct}}$, pK_a values in italics, the pH 7.4 fraction, f , of the compound in the charge state Q (indicated in parentheses), and the Abraham descriptors (α , β , π , R , V_x —alternate names in parentheses after the symbol) were calculated using the ADME Boxes V4.9 program (Pharma Algorithms). The non-italic pK_a values were taken from Avdeef (2003), and were adjusted to 0.01 M ionic strength. Ref refers to $\log P_o^{\text{PAMPA}}$ source. b: $\log P_o^{\text{PAMPA}}$ calculated by the pCEL-X v1.0 program (pION). c: This work. d: Avdeef and Tsinman (2006). e: Avdeef et al. (2004). f: Bendels et al. (2006). g: Ruell et al. (2004). h: Avdeef et al. (2005). i: Ruell et al. (2003). j: Avdeef (2005). k: Avdeef et al. (2007).

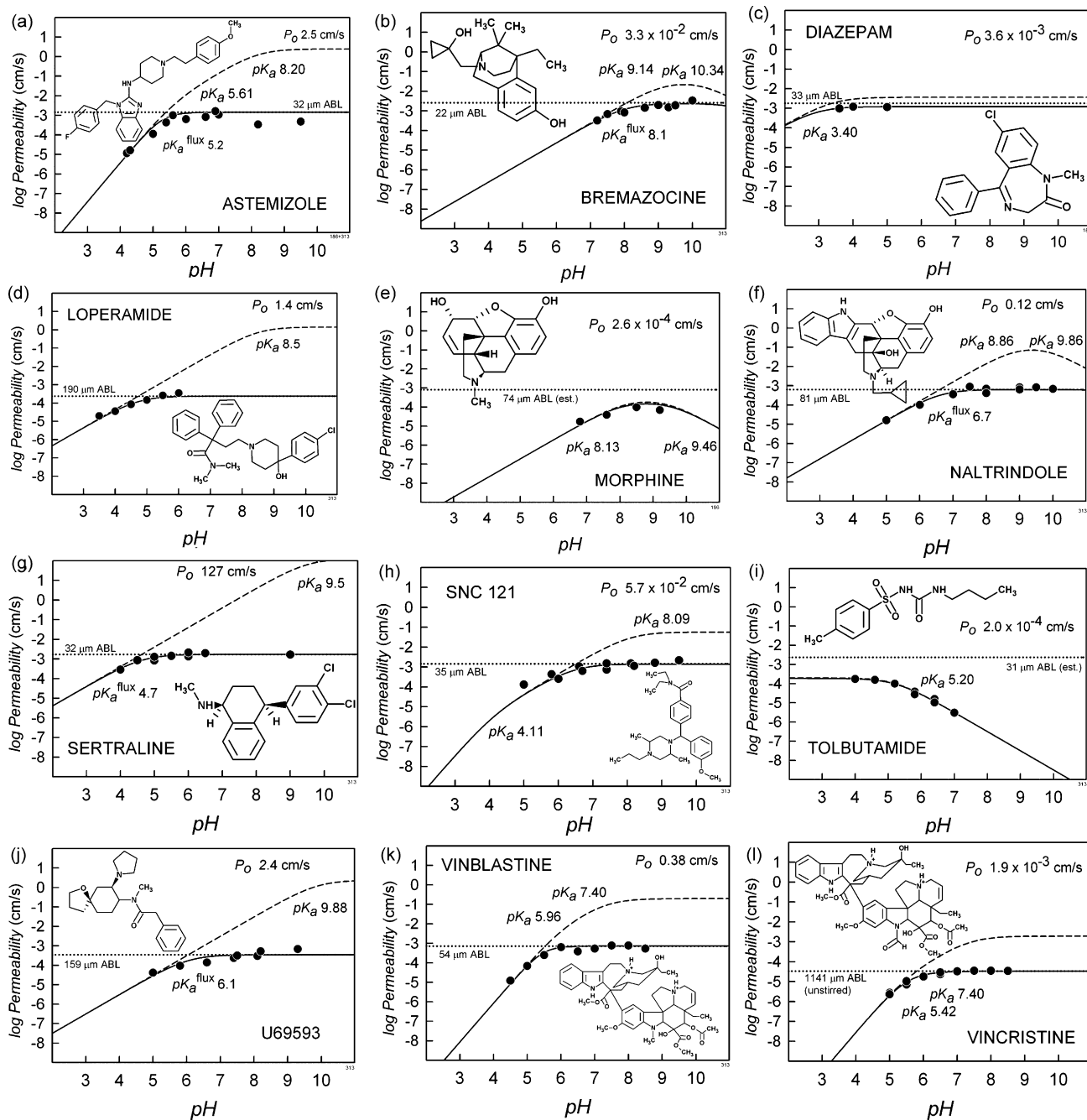


Fig. 1. The log permeability vs. pH plots of 12 of the 42 molecules measured by the PAMPA method. The pH was varied to assess the contribution of the aqueous boundary layer. The best-fits of Eq. (1) to the measured effective permeability data are represented by the solid curves, and the ABL-corrected $\log P_m$ -pH curves are represented by dashed curves. The dotted lines correspond to the $\log P_{ABL}$ values, derived from the refinement model based on Eq. (1). The maximum point in the $\log P_m$ curves corresponds to the intrinsic permeability coefficient, $\log P_o$, which characterizes the transport of the neutral form of an ionizable molecule. The intersections of the horizontal and the diagonal tangents occur at pH values corresponding to the pK_a s in the dashed curves and pK_a^{flux} in the solid curves.

may seem unnecessary, given that the environment of the BBB is very close to pH 7.4. However, the transformation is solely a computational strategy, in order to take full advantage of the Abraham descriptors. After the model was developed, the calculated intrinsic values were converted back to PS scale. In effect, by these transformations, we have adapted the Abraham molecular descriptors for charged molecules.

In addition to the LFER model, we explored how well PAMPA measurements, augmented with one (or two) of Abraham's solvation molecular descriptors, can predict $PS_{passive}$ values. The combination of measured PAMPA and a calculated LFER descrip-

tor defines the *in combo* method below. A trial-and-error testing of various combinations of one or two Abraham descriptors and PAMPA was tried, using

$$\log P_o^{BBB}(\textit{in combo}) = a_0 + a_1 \log P_o^{PAMPA} + \text{one or two Abraham descriptors} \quad (3)$$

where a_0, a_1, \dots are MLR coefficients. The usefulness of such an approach has been discussed elsewhere (Avdeef et al., 2005). Fewer MLR coefficients are necessary in Eq. (3), compared to Eq. (2), because P_o^{PAMPA} already encodes for some

of the transport characteristics common to the permeability models.

The best prediction model was validated by testing its ability to predict BBB permeability of compounds not used in the training set.

The Abraham descriptor calculation and the computational model testing used the Algorithm Builder V1.8 and ADME Boxes V4.9 computer programs (Lanevskij et al., 2008; Didziapetris et al., 2003) from Pharma Algorithms (Toronto, Canada). Since the 52-molecule test set and ten of the zwitterionic training set molecules were not available to us for PAMPA measurement, the pCEL-X v1.0 program (pION) was used to predict the missing PAMPA values.

5. Results and discussion

5.1. Pgp-deficient mouse measurements and the Pgp effect

The brain uptake values (K_{in}) for the wild-type and the Pgp-deficient mouse data, listed in Table 2, were converted to PS values (Table 3).

The PS parameter is an indicator of early access into the CNS. The short time over which the measurement is performed minimizes egress from brain to blood. As such, this parameter is independent from, and cannot predict the extent of brain distribution at steady-state, even if there is some overlap in the properties that impart high affinity for brain tissue and high passive BBB permeability. Two additional considerations further support this statement. First, the upper limit of the observed BBB permeability *in vivo* is cerebral blood flow. Therefore, compounds may have a similarly high permeability, but very different affinity for brain tissue, as illustrated by the lipophilic amine sertraline which has a very high brain volume of distribution, in comparison to the neutral compound diazepam (low to intermediate). Second, apparent permeability is the net result of passive and when applicable, carrier-mediated transport components, as indicated in Table 2. Hence a Pgp substrate may have low apparent permeability, but high affinity for brain tissue, which would obscure any underlying correlation that may have existed with respect to *passive* permeability.

The Pgp effect (Table 2) is an index of the magnitude of efflux under initial uptake conditions. It has been suggested than under initial brain uptake conditions and in the absence of plasma protein binding, the Pgp effect is an underestimate of the steady-state situation (Dagenais et al., 2001). Moreover, deriving the Pgp effect from the nonlinear PS value scale (in contrast to K_{in}) would yield much higher ratios for compounds that go from low or intermediate extraction to high extraction when efflux is removed, so it should be used to rank compounds based on their efflux potential, not in absolute terms. The compounds represented a wide range of Pgp effects ranging from no interaction (ratio of 1) to a 14-fold difference (based on K_{in} values), with K_{in} values spanning four log orders of magnitude.

5.2. PAMPA measurements

Table 1 lists the PAMPA intrinsic permeability values. The values for doxorubicin and gabapentin are poorly determined, as indicated by the standard deviations (SD). This was due to the low UV absorbance of the molecules. Fig. 1 shows the PAMPA $\log P_e$ as a function of pH for 12 of the studied molecules. Morphine, naltrindole, and bremazocine are ampholytes, and are characterized by parabolic-shaped profiles. The bases in Fig. 1 are characterized by an ascending hyperbolic curves with increasing pH.

The best-fits of Eq. (1) to the data are represented by the solid curves, and the derived lipid membrane-based $\log P_m$ -pH curves

are represented by dashed curves. The horizontal dotted lines correspond to the $\log P_{ABL}$ values, resulting from the regression analysis based on Eq. (1). The maximum point in the $\log P_m$ curves corresponds to the intrinsic permeability coefficient, $\log P_o$.

5.3. In combo PAMPA method throughput

The PAMPA method described here may appear to be low-to-medium throughput, since for most of the compounds, permeability was determined in 3–12 different pH buffers (cf., Fig. 1). This was done to reconcile the substantial difference between the aqueous boundary layer thickness in PAMPA (1500–4000 μm in unstirred plates) and in the *in situ* assay (<1 μm). Some pharmaceutical companies perform PAMPA measurements in duplicate at one pH in high-throughput assays (often without stirring). To match such a throughput, it can be proposed here that PAMPA be done at two pH values as singletons with the pH values selected to straddle the $\text{p}K_a^{\text{flux}}$ value, as described by Ruell et al. (2003). This would be sufficient to correct the data for the effects of the aqueous boundary layer, to better match the *in situ* conditions. Furthermore, if vigorous stirring were used for lipophilic compounds during the assay, the method could have up to 100-fold increase in the dynamic range of the effective permeability, with a concomitant decrease in the permeation time. Such a proposed procedure would have nearly the same workload as the commonly used high-throughput protocol, and thus could be considered high throughput. (Given that PAMPA values themselves can be predicted (e.g., pCEL-X), our proposed $\text{PS}_{\text{passive}}$ prediction model can be done entirely as a very fast *in silico* method, perhaps suitable for ranking molecules in virtual compound libraries.)

5.4. Abraham LFER and in combo PAMPA models

Comparisons of $\log P_o^{\text{BBB}}$ and $\log P_o^{\text{PAMPA}}$ were explored according to Eq. (3), using various combinations of “booster” LFER descriptors. Combinations of $\log P_o^{\text{PAMPA}}$ and the H-bond Abraham descriptors produced the lowest r^2 values. Using both α and β descriptors, the best-model multiple linear regression coefficients resulting from the search produced $r^2 = 0.80$ and $s = 0.79$ (Table 5). By comparison, the five-descriptor Abraham model yielded $r^2 = 0.69$ and $s = 0.99$ (Table 5). Inspection of the residuals suggested that the acid compounds appeared to have higher than expected passive permeability, compared to the other compounds in the training set. This may be due to the anisotropic properties of the biological membranes, consisting of various bilayer-forming amphiphilic lipids and membrane-anchored proteins. The distribution of the lipids and proteins is complex and uneven in the BBB membranes. It may be that acids, bases, neutral molecules, and zwitterions undergo passive diffusion that can best be described by different mixes of physical property descriptors. To test this hypothesis, the 130-PS training set was then partitioned into four groups: acids, bases, neutrals, and zwitterions.

The partitioned-set regression analyses led to an improved overall model, and the individual set parameters are listed in Table 5. The anions and cations had the highest correlation coefficients, 0.90 and 0.86, respectively. For the zwitterions, the 0.21 coefficient for the $\log P_o^{\text{PAMPA}}$ term was considerably lower than those of the other three groupings. Also, the contribution due to H-bond donor strength (α) varied extensively across the four types of charge groups, with neutral compounds appearing to have enhanced BBB permeability with increased H-bond donor strength, contrary to expectations. The zwitterion set had the poorest r^2 of the four groups. Abraham et al. (1997) noted that the LFER descriptors were not ideally suited for these charged species. Also, the $\log P_o^{\text{PAMPA}}$

Table 2
In situ brain perfusion data in CF-1 Pgp deficient and wild-type mice.

Compound	Wild-type K_{in} (mL/100 g/min)	SD	Pgp mutant K_{in} (mL/100 g/min)	SD	Pgp effect	T_{perf} (s)	C_{perf} (μ M)
Amitriptyline	335	44	408	45	1.2	60	1.0
Astemizole	112	5	123	20	1.1	120	0.7
Buspirone	325	30	341	8	1.0	120	1.1
Carbamazepine	173	3	184	10	1.1	120	1.1
Chlorpromazine	300	94	295	39	1.0	60	1.0
Clozapine	118	44	90	16	0.8	120	0.8
Diltiazem	65	14	130	21	2.0	180	1.2
Domperidone	3.1	1.0	9.5	2.3	3.1	180	0.9
Gabapentin	15	6	26	5	1.7	60	0.08
Galanthamine	19	5	20	2	1.1	60	0.9
Indinavir	0.52	0.12	2.4	0.5	4.6	180	0.7
p-F-D-phenylalanine	8.4	1.4	8.9	0.3	1.1	120	0.07
p-F-L-phenylalanine	127	16	142	22	1.1	60	0.09
Probenecid	0.069	0.060	0.098	0.067	1.4	180	0.9
Ritonavir	1.8	0.5	15	1	8.3	180	1.5
Saquinavir	2.9	0.4	11	1	3.8	180	1.0
Sertraline	205	29	210	58	1.0	60	1.1
Terfenadine	126	35	129	26	1.0	120	1.2
Tolbutamide	0.91	0.10	1.1	0.2	1.2	180	0.9

descriptors for many of the zwitterions were calculated using pCEL-X (whereas those of the other training-set molecules were measured), and thus are less accurate. After the *in combo* model was developed, the calculated results were transformed back to the PS scale.

Fig. 2a is a plot of observed and calculated intrinsic permeability coefficients, using the charge-partitioned models in Table 5. The combined statistics indicate $r^2 = 0.92$ and $s = 0.51$. Fig. 2b is the plot of the observed log PS as a function of the calculated values (filled circles). The transformed PS values indicated $r^2 = 0.80$ and $s = 0.51$.

5.5. External test set validation

Fig. 2 (yellow squares) shows the relationship between the *in combo* model predicted and observed test set permeability values (Summerfield et al., 2007; Gratton et al., 1997; Obradovic et al., 2007) from Table 4. For the charge-partitioned prediction, $r^2 = 0.59$, and $s = 0.67$ in the PS form (Fig. 2b), and $r^2 = 0.82$ in the intrinsic permeability form (Fig. 2a). This may be considered an adequate validation of the *in combo* training set. The largest test-set residuals were seen with AZ13007, pemoline, and lamotrigine.

5.6. Rank order model

Fig. 3 shows a rank-ordered comparison of predicted and observed *in situ* PS values, using a “low,” “intermediate,” and “high” designations. The classification boundaries were selected by inspection, and in the figure, the PS range (in 10^{-4} mL/g/s units) 0–20 defines the low class; the high class is defined by PS above 70 for the predicted set and above 150 for the observed set. The intermediate class is the zone between the high and low boundaries.

For the training set (Table 3), there were three false negatives (galanthamine, buspirone, and terfenadine) and four false positives (vinblastine, gabapentin, naltrindole, and ritonavir). This corresponds to about 18% misclassification. The origin of these discrepancies is unclear. The rest of the training set compounds (82%) were correctly classified: 37% as high, 11% as intermediate, and 34% as low.

Also included in the figure are some of the test-set molecules, indicated by italic text. These were similarly distributed as those of the training set.

The underlined compounds in Fig. 3 were those of the training set, where both the wild-type (not used in model training) and the Pgp-deficient results were predicted in the same class. Largely,

these are compounds that do not appear to be substrates of Pgp in the *in situ* method.

The seven compounds designated with an asterisk in Fig. 3 are based on wild-type PS values (not used in the training), and reveal

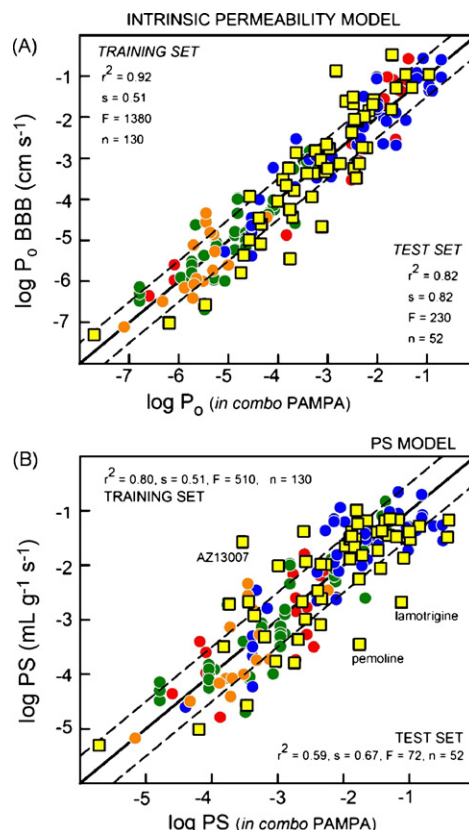


Fig. 2. Prediction of the Pgp deficient mouse brain perfusion log PS values of the 130 measurements training set (filled circles; Table 3) and the 52 compound test set (yellow squares; Table 4: data of Summerfield et al., 2007, Gratton et al., 1997, and Obradovic et al., 2007) with the *in combo* PAMPA model (Table 5). In the training set, red symbols correspond to acids (negative charged at pH 7.4), blue symbols to bases (positively charged at pH 7.4), orange to zwitterions and green to uncharged drugs. The upper frame (a) is the prediction based on the intrinsic permeability values, and the lower frame (b) has the predicted values converted back to the PS scale. (For interpretation of the references to color in this figure legend, the reader is referred to the web version of the article.)

Table 3
Training set data.

Compound	Rodent	Comment ^a	log PS(calc) (mL/g/s)	log PS(obs) (mL/g/s)	Ref	Compound	Rodent	Comment ^a	log PS(calc) (mL/g/s)	log PS(obs) (mL/g/s)	Ref
1-Aminocyclohexanecarboxylic acid	Rat	K _d	-3.5	-4.00	c	Meperidine	Mouse	mdr1a(-/-)	-0.63	-1.28	j
3-Hydroxykynurenine	Rat	K _d	-4.3	-4.49	d	Methadone	Mouse	mdr1a(-/-)	-1.47	-1.63	j
Amitriptyline	Rat	5–50 μM	-1.17	-1.05	e	Morphine	Mouse	mdr1a(-/-)	-3.38	-3.66	r
Amitriptyline	Mouse	mdr1a(-/-)	-1.17	-0.66	b	Morphine	Mouse	mdr1a(-/-)	-3.38	-3.67	j
Antipyrine	Rat		-2.81	-2.00	f	Morphine			-3.38	-3.30	s
Antipyrine	Rat		-2.81	-1.97	g	Morphine	Mouse	mdr1a(-/-)	-3.38	-3.51	n
Antipyrine	Rat		-2.81	-2.00	h	Morphine	Rat	Not saturable	-3.38	-4.23	t
Antipyrine	Rat	CsA	-2.81	-2.34	i	Morphine	Mouse	mdr1a(-/-)	-3.38	-3.49	o
Astemizole	Mouse	mdr1a(-/-)	-0.49	-1.55	b	Naltrindole	Mouse	mdr1a(-/-)	-2.33	-1.98	j
Bremazocine	Mouse	mdr1a(-/-)	-2.18	-1.89	j						
Bupirone	Mouse	mdr1a(-/-)	-2.05	-0.94	b	Naringenin	Rat	PSC833,GF120918	-1.67	-2.60	u
Carbamazepine	Rat	5–50 μM	-1.69	-1.75	e	Perphenazine	Rat	5–50 μM	-0.50	-1.27	e
Carbamazepine	Mouse	mdr1a(-/-)	-1.69	-1.26	b	p-F-Phe(D)	Mouse	mdr1a(-/-)	-3.37	-2.82	b
Cetririzine	Rat	CsA	-3.1	-3.72	i	Phenytoin			-2.12	-2.30	s
Chlorpromazine	Rat	5–50 μM	-0.80	-1.20	e	Phenytoin	Rat		-2.14	-2.20	h
Chlorpromazine	Mouse	mdr1a(-/-)	-0.80	-1.08	b	Phenytoin	Rat	5–50 μM	-2.14	-2.07	e
Cimetidine	Mouse		-3.42	-4.10	k	Prazosin	Mouse	30 μM	-2.38	-2.55	v
Cimetidine	Rat		-3.42	-4.05	k	Probenecid	Mouse	mdr1a(-/-)	-3.87	-4.79	b
Clozapine	Rat	5–50 μM	-1.02	-1.29	e	Propranolol	Rat		-2.15	-1.15	f
Clozapine	Mouse	mdr1a(-/-)	-1.02	-1.73	b	Propranolol			-2.15	-1.95	s
Colchicine	Rat	PSC833	-3.24	-3.24	l	Propranolol	Rat		-2.15	-1.20	h
Colchicine	Mouse	mdr1a(-/-)	-3.24	-3.12	m	Quercetin	Rat	PSC833, GF120918	-2.45	-3.50	u
Colchicine	Mouse	PSC833	-3.24	-3.06	n	Quetiapine	Rat	5–50 μM	-1.87	-1.33	e
Colchicine	Mouse	mdr1a(-/-)	-3.24	-3.14	o	Quinidine	Mouse	mdr1a(-/-)	-2.40	-2.13	r
Creatinine	Rat	i.v.	-3.49	-4.55	p	Quinidine	Rat	GF120918	-2.40	-2.66	w
Creatinine	Rat	i.v.	-3.49	-4.70	p	Quinine	Mouse		-2.11	-2.59	k
Deltorphan II	Mouse	mdr1a(-/-)	-4.60	-4.36	j	Quinine	Rat		-2.11	-2.63	k
Diazepam	Mouse	mdr1a(-/-)	-1.35	-1.19	q	Risperidone	Rat	5–50 μM	-2.10	-1.81	e
Diazepam	Rat	5–50 μM	-1.35	-1.37	e	Ritonavir	Mouse	mdr1a(-/-)	-2.41	-2.59	b
Digoxin	Mouse		-4.79	-4.48	k	Salicylic acid	Rat		-4.18	-3.40	h
Digoxin	Rat		-4.79	-4.30	h	Saquinavir	Mouse	mdr1a(-/-)	-3.76	-2.73	b
Digoxin	Rat		-4.79	-4.14	k	Sertraline	Rat	5–50 μM	-0.81	-0.71	e
Diltiazem	Mouse	mdr1a(-/-)	-1.68	-1.52	b	Sertraline	Mouse	mdr1a(-/-)	-0.81	-1.13	b
Diphenhydramine	Rat	CsA	-1.98	-1.21	i	SNC121	Mouse	mdr1a(-/-)	-1.39	-1.44	j
Domperidone	Mouse	mdr1a(-/-)	-3.16	-2.79	b	Sumatriptan	Rat	5–50 μM	-4.40	-4.60	e
Doxepin	Rat	5–50 μM	-1.04	-1.31	e	Terfenadine	Rat	CsA	-1.66	-1.39	i
DPDPE	Mouse	mdr1a(-/-)	-4.09	-3.97	j	Terfenadine	Mouse	mdr1a(-/-)	-1.66	-1.52	b
DPDPE	Rat		-4.09	-3.60	h	Testosterone	Rat		-1.41	-1.10	h
Estradiol	Rat		-1.37	-0.83	f	Theophylline	Mouse		-2.89	-3.26	k
Etoposide	Mouse	mdr1a(-/-)	-3.96	-3.91	x	Theophylline	Rat		-2.89	-2.90	h
Fentanyl	Mouse	mdr1a(-/-)	-1.30	-1.02	j	Theophylline	Rat		-2.89	-2.81	k
Fexofenadine	Rat	CsA	-3.78	-4.08	i	Thioridazine	Rat	5–50 μM	-0.89	-1.37	e
Flurbiprofen	Rat	Not saturable	-2.59	-1.80	y	Tiagabine	Rat	5–50 μM	-2.2	-2.46	e
Gabapentin	Rat	5–50 μM	-3.45	-2.56	e	Tolbutamide	Mouse	Saturable	-2.72	-2.60	k
Gabapentin	Mouse	mdr1a(-/-)	-3.45	-2.34	b	Tolbutamide	Mouse	mdr1a(-/-)	-2.72	-3.74	b
Galanthamine	Mouse	mdr1a(-/-)	-3.32	-2.46	b	Tolbutamide	Rat	Saturable	-2.72	-2.84	k
Glibenclamide	Mouse		-2.56	-3.27	k	U69593	Mouse	mdr1a(-/-)	-1.72	-2.01	j
Glibenclamide	Rat		-2.56	-2.77	k	Verapamil	Mouse	mdr1a(-/-)	-1.67	-1.33	r
Grepafloxacin	Rat	2 mM	-3.3	-2.91	z	Verapamil	Mouse	mdr1a(-/-)	-1.67	-1.42	m
Haloperidol	Rat	5–50 μM	-1.50	-1.46	e	Vinblastine	Mouse		-2.96	-3.32	k
HSR-903	Rat	20 mM	-3.7	-3.14	aa	Vinblastine	Rat	PSC833	-2.96	-3.36	l

Table 3 (Continued)

Compound	Rodent	Comment ^a	log PS(calc) (mL/g/s)	log PS(obs) (mL/g/s)	Ref	Compound	Rodent	Comment ^a	log PS(calc) (mL/g/s)	log PS(obs) (mL/g/s)	Ref
Hydroxyzine	Rat	CsA	-1.86	-1.41	i	Vinblastine	Mouse	mdr1a(-/-) + GF120918	-2.96	-3.12	n
Ibuprofen	Rat	K _d	-2.32	-2.03	y	Vinblastine	Rat	GF120918	-2.96	-3.27	ff
Imatinib	Mouse	mdr1a(-/-)	-2.07	-2.11	bb	Vinblastine	Mouse	mdr1a(-/-)	-2.96	-3.25	v
Indinavir	Mouse	mdr1a(-/-)	-3.52	-3.40	b	Vinblastine	Mouse	mdr1a(-/-)	-2.96	-3.31	o
Indomethacin	Rat	Not saturable	-2.36	-2.19	y	Vinblastine	Rat		-2.96	-3.49	k
Lidocaine	Rat		-1.64	-1.90	cc	Vincristine	Mouse		-4.04	-4.12	k
L-Kynurenine	Rat	K _d	-3.9	-4.16	dd	Vincristine	Mouse		-4.04	-4.00	s
L-Leucine	Rat	K _d	-3.7	-4.08	ee	Vincristine	Mouse	mdr1a(-/-)	-4.04	-3.82	n
Loperamide	Mouse	mdr1a(-/-)	-1.48	-1.66	dd	Vincristine	Mouse	mrp1(-/-)	-4.04	-4.25	x
L-Phenylalanine	Rat	K _d	-3.32	-3.74	j	Vincristine	Rat		-4.04	-3.91	ff
L-Valine	Rat	K _d	-3.7	-4.41	ee	Vincristine	Rat		-4.04	-4.10	k
M6G	Mouse	mdr1a(-/-)/glucose	-5.2	-5.17	gg	Warfarin	Mouse	Saturable	-2.29	-2.10	k
Maprotiline	Rat	5–50 μM	-2.28	-1.37	e	Warfarin	Rat	Saturable	-2.29	-1.99	k
Melphalin	Rat	K _d	-3.3	-3.28	hh	Zidovudine	Rat	i.v.	-3.07	-3.99	ii

^aK_d indicates that the PS value was the nonsaturable component taken from a Michaelis–Menten analysis; mdr1a(-/-) are Pgp-deficient (knockout) mouse data; CsA, PSC833, GF120918 indicate that efflux was inhibited by cyclosporin A, valsopodar, and elacridar, respectively; 5–50 μM, 20 mM indicate self-inhibition suppression of transporter effects; i.v. indicates intravenous injection method, for compounds not likely to be strongly bound to serum proteins, and thought to be weak substrates for transporters. b: This work. c: Aoyagi et al. (1991). d: Fukui et al. (1988). e: Summerfield et al. (2007) (please note that the original publication has an error in Table 1 *in situ* units: cm³/min are correct, not cm³–Summerfield S., private correspondence). f: Gratton et al. (1984). h: Liu et al. (2004). i: Obradovic et al. (2007). j: Dagenais et al. (2004). k: Murakami et al. (2000). l: Cisternino et al. (2003a,b). m: Dagenais (2000). n: Cisternino et al. (2001). o: Cisternino et al. (2004a,b). p: Levin (1980). q: Dagenais et al. (2001). r: Dagenais et al. (2000). s: Fenstermacher (1989). t: Bickel et al. (1996). u: Youdim et al. (2004). v: Cisternino et al. (2004a,b). w: Chen et al. (2002). x: Cisternino et al. (2003a,b). y: Parepally et al. (2006). z: Tamai et al. (1999). aa: Murata et al. (2000). ab: Bihorel et al. (2007). cc: Partridge et al. (1990). dd: Momma et al. (1987). ee: Smith et al. (1986). ff: Greig et al. (1990). gg: Bourasset et al. (2003). hh: Greig et al. (1987). ii: Wu et al. (1998).

a down-step in classification. The corresponding values of the Pgp effect ratios (Table 2) are: quinidine 14.2, ritonavir 8.3, loperamide 10.4, verapamil 6.4, diltiazem 2.0, SNC121 8.6, and methadone 2.6.

5.7. Influence of non-Pgp transport systems

Despite the fact that some training set compounds are known substrates of putative transport systems in the BBB, the model performs relatively well. Even if there is a non-Pgp efflux, or active or facilitated uptake process, the molecular properties of the compounds (and apparent permeability values) span a much broader range than the efflux ratios at the BBB. For this reason DPDPE, probenecid, gabapentin, tolbutamide, and M6G were not excluded, even though these are known to be substrates of transport systems (Deguchi et al., 1997; Sun et al., 2001; Takanaga et al., 1998; Luer et al., 1999; Uchino et al., 2002; Su et al., 1995; Ohtsuki and Terasaki, 2007). DPDPE was shown to be substrate of a saturable uptake system (Dagenais et al., 2002). Passive diffusion of DPDPE is negligible without this transport system. The estimated transport parameters, along with the highest concentration tested, 150 μM, suggest a K_{in} of 0.0862 mL/100 g/min for DPDPE, which may be reasonable to use, in place of the higher value in Table 2. Probenecid is an organic anion efflux substrate and inhibitor (Deguchi et al., 1997; Sun et al., 2001). Since gabapentin is a substrate of the large neutral amino acid transporter (LNAAT; system L), the K_{in} value in Table 2 probably overestimates passive permeability. This is nicely illustrated by the difference in BBB permeability between p-F-L- and p-F-D-phenylalanine in Table 2; due to its enantiomeric form, only the former is a recognized substrate of the LNAAT. Tolbutamide appears to be a non-Pgp efflux substrate (Takanaga et al., 1998). M6G appears to have an uptake transporter (Bourasset et al., 2003). Quantitatively, how transporters affect the blood–brain transport of these compounds in relation to intrinsic BBB permeability should be further explored as more *in vivo* data become available.

5.8. Two possible uses of the predicted PS_{passive} values

It's clear that there is a cost and speed advantage in using *in combo* PAMPA to predict BBB permeability, compared to *in vitro*, *in situ* or *in vivo* methods. Since PAMPA can only address the passive permeability component in the overall transport process, it's best to use it for virtual screening of large sets of compounds, or in a supportive role. For example, when an *in vivo*, *in situ*, or *in vitro* permeability measurement is made, it may be difficult to be certain to what extent the result represents a passive, a carrier-mediated, or an active influx/efflux process. Combining the PAMPA-predicted permeability with the more biomimetic measured values can sometimes shed light on the contributions of several components of transport, as illustrated previously (Bermejo et al., 2004; Avdeef et al., 2005). The two examples below illustrate the use of PS_{passive} determined by the *in combo* PAMPA, in the first case to indicate transporter effects (influx and efflux), and in the second case to indicate BPC classification using different parameters from those used by Kalvass et al. (2007).

5.8.1. Possible recognition of active transport

Compounds that are Pgp specific (Pgp effect > 1.5 in Table 2) will have attenuated brain uptake. Their predicted PS_{passive} will exceed the measured PS value, as illustrated by the asterisked compounds in the ranking scheme in Fig. 3. Fig. 4 shows a quantitative plot of the Pgp effect with the down-pointing (blue) triangle symbols. For this set of compounds, the vertical axis represents the measured PS values (WT), whereas the horizontal scale represents the PS_{passive} values calculated by the *in combo* PAMPA model, drawing on train-

Table 4
Test set data.

Compound	Rodent	Comment ^a	log PS(calc) (mL/g/s)	log PS(obs) (mL/g/s)	Ref	Compound	Rodent	Comment ^a	log PS(calc) (mL/g/s)	log PS(obs) (mL/g/s)	Ref
Amantadine	Rat	5–50 μM	-3.73	-2.71	b	Loxapine	Rat	5–50 μM	-1.32	-1.45	b
Amoxapine	Rat	5–50 μM	-1.37	-1.18	b	Mannitol	Rat		-4.19	-5.01	c
Atomoxetine	Rat	5–50 μM	-2.60	-1.39	b	Meprobamate	Rat	5–50 μM	-2.35	-3.09	b
AZ 11003	Rat		-0.99	-1.53	c	Mesoridazine	Rat	5–50 μM	-1.71	-1.81	b
AZ 12002	Rat		-3.82	-3.49	c	Metoclopramide	Rat	5–50 μM	-3.44	-2.67	b
AZ 13007	Rat		-3.53	-1.57	c	Midazolam	Rat	5–50 μM	-0.40	-1.17	b
AZ 22001	Rat		-3.35	-2.92	c	Mirtazapine	Rat	5–50 μM	-1.49	-1.39	b
AZ 26006	Rat		-3.20	-3.31	c	Olanzapine	Rat	5–50 μM	-0.85	-1.29	b
AZ 95005	Rat		-2.34	-2.61	c	Pemoline	Rat	5–50 μM	-1.76	-3.45	b
Brompheniramine	Rat	CsA	-1.88	-1.38	d	Pergolide	Rat	5–50 μM	-1.80	-1.00	b
Bupropion	Rat	5–50 μM	-1.82	-1.52	b	Phenelzine	Rat	5–50 μM	-2.63	-2.67	b
Chlorpheniramine	Rat	CsA	-1.98	-1.65	d	Pyrilamine	Rat	CsA	-1.88	-1.47	d
Citalopram	Rat	5–50 μM	-2.27	-1.99	b	Rizatriptan	Rat	5–50 μM	-3.03	-3.76	b
Clemastine	Rat	CsA	-1.17	-1.16	d	Selegiline	Rat	5–50 μM	-1.00	-1.39	b
Donepezil	Rat	5–50 μM	-1.89	-1.50	b	Sucrose	Rat		-5.71	-5.30	c
Ergotamine	Rat	5–50 μM	-1.44	-2.06	b	Tacrine	Rat	5–50 μM	-2.99	-2.02	b
Erythritol	Rat		-3.47	-4.57	c	Temazepam	Rat	5–50 μM	-1.42	-1.37	b
Ethanol	Rat		-1.90	-1.52	c	Thiothixene	Rat	5–50 μM	-1.29	-1.15	b
Ethosuximide	Rat	5–50 μM	-2.39	-2.47	b	Thiourea	Rat		-2.69	-3.36	c
Ethylene glycol	Rat		-2.58	-2.99	c	Thymine	Rat		-2.57	-1.93	c
Fluoxetine	Rat	5–50 μM	-1.65	-1.18	b	Trazodone	Rat	5–50 μM	-1.20	-1.47	b
Fluphenazine	Rat	5–50 μM	-1.09	-1.87	b	Trifluoperazine	Rat	5–50 μM	-1.90	-1.88	b
Isocarboxazid	Rat	5–50 μM	-1.78	-1.24	b	Urea	Rat		-2.75	-3.79	c
Isopropanol	Rat		-1.83	-1.66	c	Venlafaxine	Rat	5–50 μM	-2.34	-1.98	b
Lamotrigine	Rat	5–50 μM	-1.12	-2.67	b	Zaleplon	Rat	5–50 μM	-1.77	-2.25	b
Loratidine	Rat	CsA	-0.42	-1.49	d	Ziprasidone	Rat	5–50 μM	-1.48	-1.73	b

^aCsA indicates that Pgp efflux was inhibited by cyclosporin A; 5–50 μM indicates self-inhibition suppression of transporter effects.
b: Summerfield et al. (2007). c: Gratton et al. (1997). d: Obradovic et al. (2007).

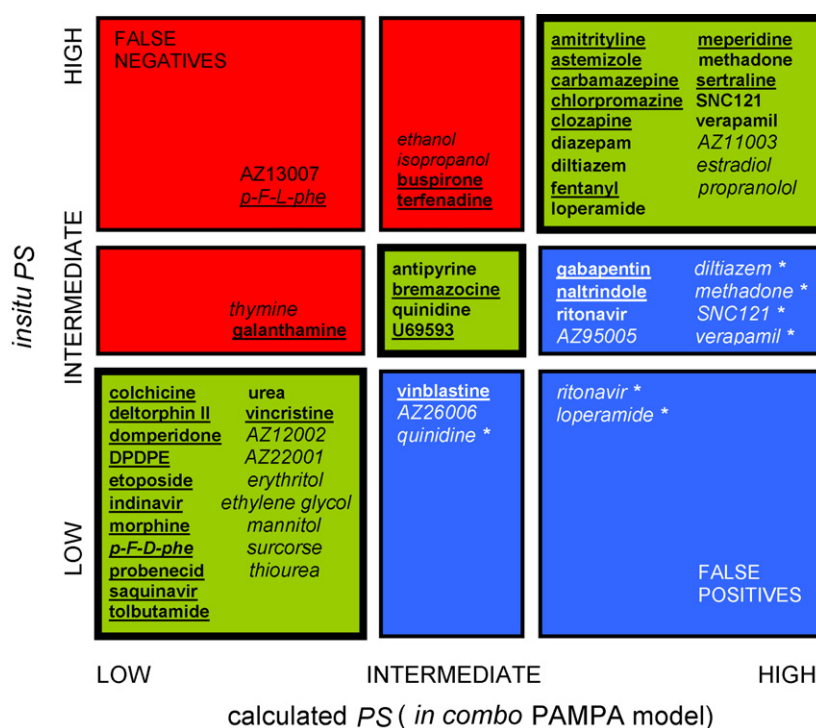


Fig. 3. Rank order comparison of *in vitro* PAMPA predicted PS values and various measured *in vivo* PS values. The vertical axis cut-off values are 20 and 150; the horizontal axis cut-offs are 20 and 70.

ing set of measurements performed with KO mice or rodents where some inhibition of transport was implemented. The further the down-triangle symbols are displaced from the solid diagonal line, the more the compound indicates a Pgp effect. The dashed diagonal lines represent a three-fold difference, where compounds falling below the threshold line show a significant Pgp effect.

Compounds that are actively uptaken in *in situ* brain perfusion measurements are indicated as upward displacements by upward-pointing (red) triangles in Fig. 4. The calculated PS_{passive} underestimates the observed permeability values. Most of the examples are amino acids. But there are some other examples, e.g., doxorubicin, daunomycin, and mitoxantrone. These compounds

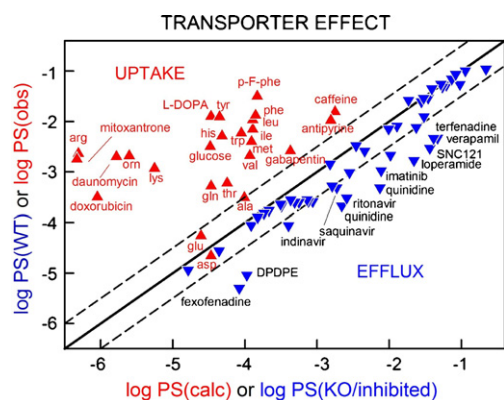


Fig. 4. Comparison of active vs. passive permeability. For the down-pointing (blue) triangle symbols, the vertical axis represents the measured PS values (WT), whereas the horizontal scale represents the PS_{passive} values calculated by the *in combo* PAMPA model. The dashed diagonal lines represent a three-fold difference, where compounds falling below the threshold line show a significant Pgp effect. Compounds that may be uptaken by some carrier-mediated (CM) process in *in situ* brain perfusion measurements are indicated as upward displacements by upward-pointing (red) triangles. For the CM set, the calculated PS_{passive} underestimates the observed permeability values. (For interpretation of the references to color in this figure legend, the reader is referred to the web version of the article.)

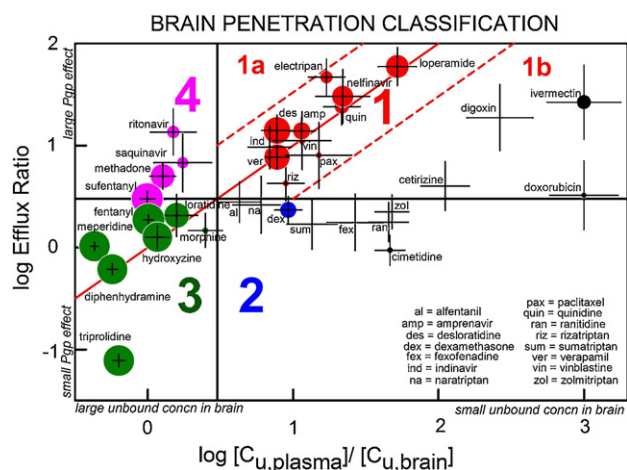


Fig. 5. The BPC scheme of Kalvass et al. (2007) with two additional parameters, PS_{passive} (this study) and $t_{1/2,eq}$ (Liu et al., 2005), superposed on the compound symbols: (a) the size of the symbols is proportional to $log PS_{\text{passive}}$; (b) the values of $log t_{1/2,eq}$ are proportionally represented by the dimensions of the “cross” symbol.

have been extensively studied in terms of efflux specificity, but very little has been reported regarding their being influx transported by a facilitated process.

5.8.2. Brain penetration classification (BPC) model enhancement

The BPC scheme described by Kalvass et al. (2007) assesses the role of Pgp and other putative processes in “impairing” (or compensating) brain penetration. Their scheme was presented in terms of a plot of the Pgp efflux ratio (ER), defined as the ratio of K_p between KO and WT mice, vs. the ratio of the unbound drug concentrations in plasma and brain tissue (the inverse of $K_{p, \text{in vitro}}^{\text{in}}$). The horizontal and vertical lines indicate an efflux ratio of 3, and ratio of unbound plasma-to-brain concentrations of 3, respectively. The different quadrants delineate various CNS penetration characteristics: (1) impaired by Pgp and/or other active process(es); (2) impaired by non-P-gp mechanism; (3) no impairment; and (4) Pgp, but no impairment due to compensatory mechanism.

Table 5
Passive BBB permeability in *in combo* model^a.

Data partitioning	a_0	a_1	a_2	a_3	r^2	s	F	n
Neutral	-1.60	0.40	+0.21	-0.75	0.78	0.51	55	50
Cations(bases)	-1.59	0.57	-0.93	-0.29	0.86	0.52	90	47
Anions(acids)	-0.02	0.50	-0.48	-0.33	0.90	0.66	37	17
Zwitterions	-3.52	0.21	-0.69	-0.17	0.66	0.54	8	16

^a $log P_0^{BBB}$ (in *in combo*) = $a_0 + a_1 log P_0^{PAMPA} + a_2\alpha + a_3\beta$. The linear correlation coefficient is r^2 ; s = standard deviation; F = “ F ” statistic; n = number of training set compounds in the group. Data partitioning is determined on the basis of predominant charge at pH 7.4 (cf., Table 1). When all compounds are combined in one set, the calculated result is $log P_0^{BBB}$ (in *in combo*) = $-1.20 + 0.50 log P_0^{PAMPA} + 0.365\alpha - 0.76\beta$; $r^2 = 0.80$, $s = 0.79$, $F = 167$. The Abraham model produces $log P_0^{BBB}$ (LFER) = $-3.66 - 0.53\alpha - 3.23\beta + 0.50\pi + 0.15R + 1.69V_x$; $r^2 = 0.69$, $s = 0.99$, $F = 55$.

Their BPC plot for 34 compounds is reproduced in Fig. 5, but with two additional parameters, PS_{passive} (determined by *in combo* PAMPA) and $t_{1/2,eq}$ (calculated from PS_{passive} and $f_{u,brain}$ using the method and data from Liu et al., 2005) superposed on the compound symbols: (a) the size of the symbols is proportional to $log PS_{\text{passive}}$; (b) the values of $log t_{1/2,eq}$ are proportionally represented by the “cross” symbol, with the largest cross symbol representing 624 min (ivermectin) and the smallest cross symbol representing 2 min (meperidine). We acknowledge that PS_{passive} is an overestimate of the true *in vivo* permeability for efflux substrates, which at first consideration appears to bias the estimate of $t_{1/2,eq}$ by shortening it. However, while a decrease in BBB permeability due to Pgp efflux may be expected intuitively to result in lengthening of $t_{1/2,eq}$ modeling of blood–brain transport in this specific case suggests that the effect would be more or less reversed depending on the magnitude of the increase in blood-to-brain egress (Syvänen et al., 2006). Although the relative balance between these two parameters is unknown for the Pgp substrates in Fig. 5, we still considered the exercise conceptually useful, especially to qualify Class 3 compounds.

In the BPC plot in Fig. 5, Classes 3 and 4 on the left side are characterized by unbound drug concentration in the brain of about 30% or more than in the blood. These two classes may be designated “CNS+”. Conversely, the other classes on the right side of the plot can be designated “CNS–” for the purpose of the present discussion. Di et al. (2003) were able to differentiate CNS+ from CNS– groups using PAMPA. In the present study, PS_{passive} was used to define class boundaries in the BPC scheme in Fig. 5.

Inspection of Fig. 5 indicates that the most intrinsically permeable compounds are associated with BPC Class 3 (no impairment to brain penetration). However, intermediate to high PS_{passive} values also are associated with Class 1 (Pgp impaired penetration), simply reflecting that PS_{passive} is not a predictor of Pgp efflux ratio. However, it should be noted that for compounds that can bind to Pgp, the residence time in the cell membrane (a direct function of PS_{passive}) must be sufficient for an interaction to occur and result in significant efflux. For instance, although some high permeability compounds may display affinity for Pgp and act as inhibitors, they display little or no apparent efflux due to passive escape. The three-fold off-diagonal (outside of the dashed-line boundary in Fig. 5) compounds generally have very low PS_{passive} , suggesting it is also a contributor to poor CNS penetration. Evidently PS_{passive} alone cannot differentiate impaired from non-impaired compounds in the BPC scheme. The average values of PS_{passive} , $f_{u,brain}$ and $t_{1/2,eq}$ (a combination of the first 2 parameters) for the 34 compounds in Fig. 5 were compiled for each of the BPC groups, along with the 68% probability ranges, and are listed in Table 6. Conceptually, $t_{1/2,eq}$ is shortest when both permeability and free fraction in brain are high. As mentioned above, there

Table 6
Brain penetration classification (BPC) and the rate of penetration^a.

BPC class	PS (mL/g/s)		$f_{u,br} \times 100\%$		$t_{1/2,eq}$ (min)		BBB penetration
1	68	(2–160)	6	(0.05–16)	70	(8–170)	Impaired by Pgp
1b	6	(0.5–16)	2	(0.01–6)	340	(110–570)	Impaired by Pgp + other
2	5	(0.1–15)	39	(10–68)	58	(5–110)	Impaired by non-Pgp
3	430	(180–690)	19	(0.2–41)	10	(2–24)	Not impaired
4	200	(12–500)	2	(0.4–3.4)	58	(12–500)	Not impaired—compensating mechanism

^a The four classes in the extent of brain penetration, according to Kalvass et al. (2007). Listed for each of the three properties are the mean values and the 68%-probability range, based on the 34-compound set from Kalvass et al. (2007).

is some overlap in the molecular properties that govern the latter two parameters, but that can be obscured by active efflux or uptake. There cannot be permeability if the compound is unable to partition in cell membranes, which is to a large extent analogous to partitioning in brain tissue. The optimal CNS candidate has good permeability, moderate affinity for brain tissue and no efflux, which appears to be the hallmark of Class 3 compounds. One notes that Class 1 (impaired) and Class 3 (unimpaired) have large differences in the average $PS_{passive}$ (68 vs. 430, 10^{-4} mL/g/s units), perhaps suggesting that these compounds have a slightly longer residence time in the luminal cell membrane that maximizes interactions with Pgp as discussed above. From the PS parameter ranges, 170 appears to be a good boundary value to differentiate the two classes. Another important difference between the two classes is the value of brain tissue binding. This binding in Class 1 compounds is notably greater (average $f_{u,brain} = 6\%$) than those in Class 3 (average $f_{u,brain} = 19\%$), but the two ranges overlap significantly. Perhaps these two measured quantities could be used in drug discovery in the following way: a compound is very likely not to be brain penetration impaired (Class 3) if $PS_{passive} > 170 \times 10^{-4}$ mL/g/s and $f_{u,brain} > 16\%$. Class 4 (unimpaired due to compensation mechanisms) and Class 3 (unimpaired) both have high $PS_{passive}$, with considerable overlap in permeability values. However, the average values of $f_{u,brain}$ for the two classes are quite different. In such a comparison, a test compound is more likely to be Class 4 than Class 3 if $f_{u,brain} < 3.4\%$ and $PS_{passive} < 180 \times 10^{-4}$ mL/g/s. Classes 2 and 1b are characterized by low values of $PS_{passive}$, again suggesting that this parameter contributes at least in part to poor brain penetration. However, the values of $f_{u,brain}$ are dramatically different in the two classes (Table 5).

Although the overall number of compounds used to create the BPC probably has to be increased in order to confirm the rules we suggest, the empirical observations above may be useful in drug discovery applications, since $PS_{passive}$ (PAMPA) and $f_{u,brain}$ (brain homogenate dialysis) can be measured at high-throughput speeds at a relatively low cost.

6. Conclusion

There exist multiple and complementary methodologies to study BBB transport and distribution in various brain compartments. The ability to cross the BBB at a sufficiently high rate (i.e., permeability) to avoid excessive blood–brain equilibration delays, unhindered by efflux processes, is a pre-requisite for CNS active compounds to distribute to brain, and exert their pharmacological action while maximizing peripheral safety margins. We used a mouse brain perfusion technique to estimate the BBB permeability of drugs and drug-like compounds with a wide range of molecular properties, and enhanced this dataset with published rodent values. We have demonstrated that the *in combo* PAMPA method, trained with 130 *in situ* P-glycoprotein deficient/inhibited rodent brain perfusion data, was able to predict 82% of the variance in the intrinsic BBB permeability of 52 external test compounds, whose permeabil-

ity values were not used in the original training. Our investigation, based on 182 rodent brain perfusion results, is one of the largest PS-based published study to date used to develop a BBB permeability prediction model. The passive permeability predictions allowed us to further qualify and understand the brain penetration classification suggested by other investigators. Based on correlation plots (Fig. 2), the rank order comparisons (Fig. 3) and the transporter effect considerations (Fig. 4), we conclude that we have met the objectives of our study: to develop a practical, low-cost, and fast quantitative method which could be used for early passive BBB permeability screening, and for assisting medicinal chemists with structure modification to improve the BBB permeability of test compounds downstream in the CNS drug discovery process.

Acknowledgements

We thank Debra McCombs, Julie Zalikowski and Cindy Shen for their skilled bioanalytical support at AstraZeneca. Discussions with, and suggestions from, Drs. Joan Abbott, David Begley, and Sarah Thomas of King's College London, Khanh Bui and Mary Bock from AstraZeneca, and Michel Demeule at UQAM, Per Nielson from pION, are gratefully acknowledged. Part of this work was supported by Grant Number R44MH75211 from the National Institutes of Health (to pION). The content is solely the responsibility of the authors and does not necessarily represent the official views of the National Institute of Mental Health or the National Institutes of Health.

References

- Abbott, N.J., 2007. *In vitro* models for examining and predicting brain uptake of drugs. In: Testa, B., van de Waterbeemd, H. (Eds.), *Comprehensive Medicinal Chemistry II*, vol. 5, ADME-Tox Approaches. Elsevier, Amsterdam, pp. 301–320.
- Abraham, M.H., Takács-Novák, K., Mitchell, R.C., 1997. On the partition of ampholytes: application to blood–brain distribution. *J. Pharm. Sci.* 86, 310–315.
- Abraham, M.H., 2004. The factors that influence permeation across the blood–brain barrier. *Eur. J. Med. Chem.* 39, 235–240.
- Aoyagi, M., Agranoff, B.W., Washburn, L.C., Smith, Q.R., 1988. Blood–brain barrier transport of 1-aminocyclohexanecarboxylic acid, a nonmetabolic amino acid for *in vivo* studies of brain transport. *J. Neurochem.* 50, 1220–1226.
- Avdeef, A., 2003. *Absorption and Drug Development*. Wiley–Interscience, pp. 116–246.
- Avdeef, A., Nielsen, P., Tsinman, O., 2004. PAMPA—a drug absorption *in vitro* model. 11. Matching the *in vivo* aqueous boundary layer by individual-well stirring in microtitre plates. *Eur. J. Pharm. Chem.* 22, 365–374.
- Avdeef, A., Artursson, P., Neuhoff, S., Lazorova, L., Gräsjö, J., Tavelin, S., 2005. Caco-2 permeability of weakly basic drugs predicted with the Double-Sink PAMPA pK_{flux} method. *Eur. J. Pharm. Sci.* 24, 333–349.
- Avdeef, A., 2005. The rise of PAMPA. *Expert Opin. Drug Metab. Toxicol.* 1, 325–342.
- Avdeef, A., Tsinman, O., 2006. PAMPA—a drug absorption *in vitro* model. 13. Chemical selectivity due to membrane hydrogen bonding: in combo comparisons of HDM-, DOPC-, and DS-PAMPA. *Eur. J. Pharm. Sci.* 28, 43–50.
- Avdeef, A., Bendels, S., Di, L., Faller, B., Kansy, M., Sugano, K., Yamauchi, Y., 2007. PAMPA—a useful tool in drug discovery. *J. Pharm. Sci.* 96, 2893–2909.
- Bendels, S., Tsinman, O., Wagner, B., Lipp, D., Parilla, I., Kansy, M., Avdeef, A., 2006. PAMPA–excipient classification gradient map. *Pharm. Res.* 23, 2525–2535.
- Bendels, S., Kansy, M., Wagner, B., Huwyler, J., 2008. *In silico* prediction of brain and CSF permeation of small molecules using PLS regression models. *Eur. J. Med. Chem.* 43, 1581–1592.
- Benveniste, H., Huttemeier, P.C., 1990. Microdialysis—theory and applications. *Prog. Neurobiol.* 35, 195–215.
- Bermejo, M., Avdeef, A., Ruiz, A., Nalda, R., Ruell, J.A., Tsinman, O., González, I., Fernández, C., Sánchez, G., Garrigues, T.M., Merino, V., 2004. PAMPA—a drug absorption

- in vitro* model. 7. Comparing rat *in situ*, Caco-2, and PAMPA permeability of fluoroquinolones. *Eur. J. Pharm. Sci.* 21, 429–441.
- Bickel, U., Schumacher, O.P., Kang, Y.-S., Voigt, K., 1996. Poor permeability of morphine 3-glucuronide and morphine 6-glucuronide through the blood–brain barrier in the rat. *J. Pharmacol. Exp. Ther.* 278, 107–113.
- Bihorel, S., Camenisch, G., Lemaire, M., Scherrmann, J.-M., 2007. Modulation of the brain distribution of imatinib and its metabolites in mice by valsopodar, zosuquidar and elacridar. *Pharm. Res.* 24, 1720–1728.
- Bourasset, F., Cisternino, S., Tamsamani, J., Scherrmann, J.M., 2003. Evidence for an active transport of morphine-6- β -D-glucuronide but not P-glycoprotein-mediated at the blood–brain barrier. *J. Neurochem.* 86, 1564–1567.
- Cecchelli, R., Berezowski, V., Lundquist, S., Culot, M., Renftel, M., Dehouck, M.-P., Fenart, L., 2007. Modeling of the blood–brain barrier in drug discovery and development. *Nat. Rev./Drug Discov.* 6, 650–661.
- Chen, W., Yang, J.Z., Anderson, R., Nielsen, L.H., Borchardt, R.T., 2002. Evaluation of the permeability characteristics of a model opioid peptide, H-Tyr-D-Ala-Gly-Phe-D-Leu-OH (DADLE), and its cyclic prodrugs across the blood–brain barrier using an *in situ* perfused rat brain model. *J. Pharmacol. Exp. Ther.* 303, 849–857.
- Cisternino, S., Rousselle, C., Dagenais, C., Scherrmann, J.-M., 2001. Screening of multidrug-resistance sensitive drugs by *in situ* brain perfusion in P-glycoprotein deficient mice. *Pharm. Res.* 18, 183–190.
- Cisternino, S., Rousselle, C., Debray, M., Scherrmann, J.-M., 2003a. *In vivo* saturation of the transport of vinblastine and colchicines by P-glycoprotein at the rat blood–brain barrier. *Pharm. Res.* 20, 1607–1611.
- Cisternino, S., Rousselle, C., Lorico, A., Rappa, G., Scherrmann, J.-M., 2003b. Apparent lack of mrp1-mediated efflux at the luminal side of mouse blood–brain barrier endothelial cells. *Pharm. Res.* 20, 904–909.
- Cisternino, S., Mercier, C., Bourasset, F., Rouse, F., Scherrmann, J.-M., 2004a. Expression, up-regulation, and transport activity of the multidrug-resistance protein Abcg2 at the mouse blood–brain barrier. *Cancer Res.* 64, 3296–3301.
- Cisternino, S., Rousselle, C., Debray, M., Scherrmann, J.-M., 2004b. *In situ* transport of vinblastine and selected P-glycoprotein substances: implications for drug–drug interactions at the mouse blood–brain barrier. *Pharm. Res.* 21, 1382–1389.
- Clark, D.E., 2003. *In silico* prediction of blood–brain barrier permeation. *Drug Discov. Today* 8, 927–933.
- Dagenais, C., 2000. Blood–brain barrier transport of opioids and selected substrates: variable modulation of brain uptake by P-glycoprotein and countervectorial transport systems for the model opioid peptide [D-Pen^{2,5}]-Enkephalin. Ph.D. Dissertation. Univ. of North Carolina.
- Dagenais, C., Rousselle, C., Pollack, G.M., Scherrmann, J.-M., 2000. Development of an *in situ* mouse brain perfusion model and its application to mdr1a P-glycoprotein-deficient mice. *J. Cereb. Blood Flow Metab.* 20, 381–386.
- Dagenais, C., Zong, J., Ducharme, J., Pollack, G.M., 2001. Effect of mdr1a P-glycoprotein gene disruption, gender, and substrate concentration on brain uptake of selected compounds. *Pharm. Res.* 18, 957–963.
- Dagenais, C., Ducharme, J., Pollack, G.M., 2002. Interaction of nonpeptidic δ agonists with P-glycoprotein by *in situ* mouse brain perfusion: LC–MS analysis and internal standard strategy. *J. Pharm. Sci.* 91, 244–252.
- Dagenais, C., Graff, C.L., Pollack, G.M., 2004. Variable modulation of opioid brain uptake by P-glycoprotein in mice. *Biochem. Pharmacol.* 67, 269–276.
- Dagenais, C., Ducharme, J., Pollack, G.M., 2005. Uptake and efflux of the peptidic delta-opioid receptor agonist [d-penicillamine^{2,5}]-enkephalin at the murine blood–brain barrier by *in situ* perfusion. *Neurosci. Lett.* 301, 155–158.
- Deguchi, Y., Nozawa, K., Yamada, S., Yokoyama, Y., Kimura, R., 1997. Quantitative evaluation of brain distribution and blood–brain barrier efflux transport of probenecid in rats by microdialysis: possible involvement of the monocarboxylic acid transport system. *J. Pharmacol. Exp. Ther.* 290, 551–560.
- Di, L., Kerns, E.H., Fan, K., McConnell, O.J., Carter, G.T., 2003. High throughput artificial membrane permeability assay for blood–brain barrier. *Eur. J. Med. Chem.* 38, 223–232.
- Di, L., Kerns, E.H., Bezar, I.F., Petusky, S.L., Huang, Y., 2009. Comparison of blood–brain barrier permeability assays: *in situ* brain perfusion, MDR1-MDCKII and PAMPA-BBB. *J. Pharm. Sci.* (epub October 2008: doi:10.1002/jps.21580).
- Didziapetris, R., Japertas, P., Avdeef, A., Petrauskas, A., 2003. Classification analysis of P-glycoprotein substrate specificity. *J. Drug Target.* 11, 391–406.
- Fenstermacher, J.D., 1989. Pharmacology of the BBB. In: Neuwelt, E.A. (Ed.), *Implications of the BBB and its Manipulation*, vol. 1. Plenum Press, New York, pp. 137–155.
- Fridén, M., Gupta, A., Antonsson, M., Bredberg, U., Hammarlund-Udenaes, M., 2007. *In vitro* methods for estimating unbound drug concentrations in the brain interstitial and intracellular fluids. *Drug Metab. Dispos.* 35, 1711–1719.
- Fukui, S., Schwarcz, R., Rapoport, S.I., Takada, Y., Smith, Q.R., 1991. Blood–brain barrier transport of kynurenes: implications for brain synthesis and metabolism. *J. Neurochem.* 56, 2007–2017.
- Garberg, P., Ball, M., Borg, N., Cecchelli, R., Fenart, L., Hurst, R.D., Lindmark, T., Mabondzo, A., Nilsson, J.E., Raub, T.J., Stanimirovic, D., Terasaki, T., Osterberg, J.O., Osterberg, T., 2005. *In vitro* models for the blood–brain barrier. *Toxicol. In Vitro* 19, 299–334.
- Garg, P., Verma, J., 2006. *In silico* prediction of blood–brain barrier permeability: an artificial neural network model. *J. Chem. Inf. Model.* 46, 289–297.
- Gratton, J.A., Abraham, M.H., Bradbury, M.W., Schadka, H., 1997. Molecular factors influencing drug transfer across the blood–brain barrier. *J. Pharm. Pharmacol.* 49, 1211–1216.
- Greig, N.H., Momma, S., Sweeney, D.J., Smith, Q.R., Rapoport, S.I., 1987. Facilitated transport of melphalan at the rat blood–brain barrier by the large neutral amino acid carrier system. *Cancer Res.* 47, 1571–1576.
- Greig, N.H., Soncrant, T., Shetty, H.U., Momma, S., Smith, Q.R., Rapoport, S.I., 1990. Brain uptake and anticancer activities of vincristine and vinblastine are restricted by their low cerebrovascular permeability and binding to plasma constituents in rat. *Cancer Chemother. Pharmacol.* 26, 263–268.
- Hammarlund-Udenaes, M., Fridén, M., Syvänen, S., Gupta, A., 2008. On the rate and extent of drug delivery to the brain. *Pharm. Res.* 25, 1737–1750.
- Hitchcock, S.A., 2008. Blood–brain barrier permeability considerations for CNS-targeted compound library design. *Curr. Opin. Chem. Biol.* 12, 1–6.
- Jeffrey, P., Summerfield, S.G., 2007. Challenges for blood–brain barrier (BBB) screening. *Xenobiotica* 37, 1135–1151.
- Kalvass, J.C., Maurer, T.S., 2002. Influence of nonspecific brain and plasma binding on CNS exposure: implications for rational drug discovery. *Biopharm. Drug Dispos.* 23, 327–338.
- Kalvass, J.C., Maurer, T.S., Pollack, G.M., 2007. Use of plasma and brain unbound fractions to assess the extent of brain distribution of 34 drugs: comparison of unbound concentration ratios to P-glycoprotein efflux ratios. *Drug Metab. Dispos.* 35, 660–666.
- Kansy, M., Senner, F., Gubernator, K., 1998. Physicochemical high throughput screening: parallel artificial membrane permeability assay in the description of passive absorption processes. *J. Med. Chem.* 41, 1007–1010.
- Kortagere, S., Chekmarev, D., Welsh, W.J., Ekins, S., 2008. New predictive models for blood–brain barrier permeability of drug-like molecules. *Pharm. Res.* 25, 1836–1845.
- Lanevskij, K., Japertas, P., Didziapetris, R., Petrauskas, A., 2008. Ionization-specific prediction of blood–brain barrier permeability. *J. Pharm. Sci.* 98, 122–134.
- Levin, V.A., 1980. Relationship of octanol/water partition coefficient and molecular weight to rat brain capillary permeability. *J. Med. Chem.* 23, 682–684.
- Liu, X., Tu, M., Kelley, R.S., Chen, C., Smith, B.J., 2004. Development of a computational approach to predict blood–brain barrier permeability. *Drug Metab. Dispos.* 32, 132–139.
- Liu, X., Smith, B.J., Chen, C., Callegari, E., Becker, S.L., Chen, X., Cianfrogna, J., Doran, A.C., Doran, S.D., Gibbs, J.P., Hosea, N., Liu, J., Nelson, F.R., Szewc, M.A., van Deusen, J., 2005. Use of a physiologically based pharmacokinetic model to study the time to reach brain equilibrium: an experimental analysis of the role of blood–brain barrier permeability, plasma protein binding, and brain tissue binding. *J. Pharmacol. Exp. Ther.* 313, 1254–1262.
- Liu, X., Chen, C., Smith, B.J., 2008. Progress in brain penetration in drug discovery and development. *J. Pharmacol. Exp. Ther.* 325, 349–356.
- Luer, M.S., Hamani, C., Dujovny, M., Gidal, B., Cwik, M., Deyo, K., Fischer, J.H., 1999. Saturable transport of gabapentin at the blood–brain barrier. *Neuro. Res.* 21, 559–562.
- Mahar Doan, K.M., Wring, S.A., Shampine, L.J., Jordan, K.H., Bishop, J.P., Kratz, J., Yang, E., Serabjit-Singh, C.J., Adkinson, K.K., Polli, J.W., 2004. Steady-state brain concentration of antihistamines in rats: interplay of membrane permeability, P-glycoprotein efflux and plasma protein binding. *Pharmacology* 72, 92–98.
- Martin, I., 2004. Prediction of blood–brain barrier penetration: are we missing the point? *Drug Discov. Today* 9, 161–162.
- Maurer, T.S., DeBartolo, D.B., Tess, D.A., Scott, D.O., 2005. Relationship between exposure and nonspecific binding of thirty-three central nervous system drugs in mice. *Drug Metab. Dispos.* 33, 175–181.
- Momma, S., Aoyagi, M., Rapoport, S.I., Smith, Q.R., 1987. Phenylalanine transport across the blood–brain barrier as studied with the *in situ* brain perfusion technique. *J. Neurochem.* 48, 1291–1300.
- Murakami, H., Takanaga, H., Matsuo, H., Ohtani, H., Sawada, Y., 2000. Comparison of blood–brain barrier permeability in mice and rats using *in situ* brain perfusion technique. *Am. J. Physiol. Heart Circ. Physiol.* 279, H1022–H1029.
- Murata, M., Tamai, I., Kato, H., Nagata, O., Kato, H., Tsuji, A., 1999. Efflux transport of a new quinolone antibacterial agent, HSR-903, across the blood–brain barrier. *J. Pharmacol. Exp. Ther.* 290, 51–57.
- Obradovic, T., Dobson, G.G., Shingaki, T., Kungu, T., Hidalgo, I.J., 2007. Assessment of the first and second generation antihistamines brain penetration and the role of P-glycoprotein. *Pharm. Res.* 24, 318–327.
- Ohno, K., Pettigrew, K.D., Rapoport, S.I., 1978. Lower limits of cerebrovascular permeability to nonelectrolytes in the conscious rat. *Am. J. Physiol.* 235, H299–H307.
- Ohtsuki, S., Terasaki, T., 2007. Contribution of carrier-mediated transport systems to the blood–brain barrier as a supporting and protecting interface for the brain; importance for CNS drug discovery and development. *Pharm. Res.* 24, 1745–1758.
- Partridge, W.M., Triguero, D., Yang, J., Cancilla, P.A., 1990. Comparison of *in vitro* and *in vivo* models of drug transcytosis through the blood–brain barrier. *J. Pharmacol. Exp. Ther.* 253, 884–891.
- Partridge, W.M., 2007. Blood–brain barrier delivery. *Drug Discov. Today* 12, 54–61.
- Parepally, J.M.R., Mandula, H., Smith, Q.R., 2006. Brain uptake of nonsteroidal anti-inflammatory drugs: ibuprofen, flurbiprofen, and indomethacin. *Pharm. Res.* 23, 873–881.
- Reichel, A., 2009. Addressing CNS penetration in drug discovery: a paradigm in change. In: *Proceedings–PhysChem and ADMET Profiling in Drug Research The 4th LogP Symposium*, 8–11 February, Zurich.
- Ruell, J.A., Tsinman, K.L., Avdeef, A., 2003. PAMPA—a drug absorption *in vitro* model. 5. Unstirred water layer in iso-pH mapping assays and pK_a^{flux} -optimized design (pOD-PAMPA). *Eur. J. Pharm. Sci.* 20, 393–402.

- Ruell, J.A., Tsinman, O., Avdeef, A., 2004. Acid–base cosolvent method for determining aqueous permeability of amiodarone, itraconazole, tamoxifen, terfenadine and other very insoluble molecules. *Chem. Pharm. Bull.* 52, 561–565.
- Smith, Q.R., Takasato, Y., 1986. Kinetics of amino acid transport at the blood–brain barrier studied using an *in situ* brain perfusion technique. *Ann. N.Y. Acad. Sci.* 481, 186–201.
- Su, T.Z., Lunney, E., Campbell, G., Oxender, D.L., 1995. Transport of gabapentin, a gamma-amino acid drug, by system I alpha-amino acid transporters: a comparative study in astrocytes, synaptosomes, and CHO cells. *J. Neurochem.* 64, 2125–2131.
- Summerfield, S.G., Stevens, A.J., Cutler, L., del Carmen Osima, L., Hammond, B., Tang, A.P., Hersey, A., Spalding, D.J., Jeffrey, P., 2006. Improving the *in vitro* prediction of *in vivo* CNS penetration: integrating permeability, Pgp efflux and free fractions in blood and brain. *J. Pharmacol. Exp. Ther.* 316, 1282–1290.
- Summerfield, S.G., Read, K., Begley, D.J., Obradovic, T., Hidalgo, I.J., Coggon, S., Lewis, A.V., Porter, R.A., Jeffrey, P., 2007. Central nervous system drug disposition: the relationship between *in situ* brain permeability and brain free fraction. *J. Pharmacol. Exp. Ther.* 322, 205–213.
- Sun, H., Miller, D.W., Elmquist, W.F., 2001. Effect of probenecid on fluorescein transport in the central nervous system using *in vitro* and *in vivo* models. *Pharm. Res.* 18, 1542–1549.
- Syvänen, S., Xie, R., Sahin, S., Hammarlund-Udenaes, M., 2006. Pharmacokinetic consequences of active drug efflux at the blood–brain barrier. *Pharm. Res.* 23, 705–717.
- Takanaga, H., Murakami, H., Koyabu, N., Matsuo, H., Naito, M., Tsuruo, T., Sawada, Y., 1998. Efflux transport of tolbutamide across the blood–brain barrier. *J. Pharm. Pharmacol.* 50, 1027–1033.
- Takasato, Y., Rapoport, S.L., Smith, Q.R., 1984. An *in situ* brain perfusion technique to study cerebrovascular transport in the rat. *Am. J. Physiol.* 247, H484–H493.
- Tamai, I., Yamashita, J., Kido, Y., Ohnari, A., Sai, Y., Shima, Y., Naruhashi, K., Koizumi, S., Tsuji, A., 2000. Limited distribution of new quinolone antibacterial agents into brain caused by multiple efflux transporters at the blood–brain barrier. *J. Pharmacol. Exp. Ther.* 295, 146–152.
- Terasaki, T., Ohtsuki, S., Hori, S., Takanaga, H., Nakashima, E., Hosoya, K.-I., 2003. New approaches to *in vitro* models of blood–brain barrier drug transport. *Drug Discov. Today* 8, 944–954.
- Uchino, H., Kanai, Y., Kim, K., Wempe, M.F., Chairoungdua, A., Morimoto, E., Anders, M.W., Endou, H., 2002. Transport of amino acid-related compounds mediated by L-type amino acid transporter 1 (LAT1): insights into the mechanisms of substrate recognition. *Mol. Pharmacol.* 61, 729–737.
- Wan, H., Rehngren, M., Giordanetto, F., Bergström, F., Tunek, A., 2007. High-throughput screening of drug–brain tissue binding and *in silico* prediction for assessment of central nervous system drug delivery. *J. Med. Chem.* 50, 4606–4615.
- Weksler, B.B., Subileau, E.A., Perrière, N., Charneau, P., Holloway, K., Leveque, M., Tricôire-Leignel, H., Nicotra, A., Bourdoulous, S., Turowski, P., Male, D.K., Roux, F., Greenwood, J., Romero, I.A., Couraud, P.O., 2005. Blood–brain barrier-specific properties of a human adult endothelial cell line. *FASEB J.* 19, 1872–1874.
- Wu, D., Clement, J.G., Pardridge, W.M., 1998. Low blood–brain barrier permeability to azidothymidine (AZT), 3TC, and thymidine in the rat. *Brain Res.* 791, 313–316.
- Youdim, K.A., Avdeef, A., Abbott, N.J., 2003. *In vitro* trans-monolayer permeability calculations: often forgotten assumptions. *Drug Discov. Today* 8, 997–1003.
- Youdim, K.A., Kaiser, M.Z., Begley, D.J., Rice-Evans, C.A., Abbott, N.J., 2004. Flavonoid permeability across an *in situ* model of the blood–brain barrier. *Free Radic. Biol. Med.* 36, 592–604.
- Zhang, L., Zhu, H., Oprea, T.I., Golbraikh, A., Tropsha, A., 2008. QSAR modelling of the blood–brain barrier permeability for diverse organic compounds. *Pharm. Res.* 25, 1902–1914.

Glossary

ER: efflux ratio

K_p : total brain/plasma concentration ratio at steady state; $K_p = AUC_{tot,brain} / AUC_{tot,plasma}$; sometimes a single time point determination at distribution equilibrium is used, with the parameter called log BB

$K_{p,uu}$: *in vivo* unbound brain ISF/unbound plasma concentration ratio at steady state = ratio of sum of all passive and active influx clearances, minus possible active efflux clearances, divided by the sum of all elimination clearances from the brain (passive, active BBB transport, metabolism, and elimination via ISF bulk flow); $K_{p,uu} = AUC_{u,brainISF} / AUC_{u,plasma}$

$K_{p,uu}^{in vitro}$: *in vitro* unbound blood-free brain/unbound plasma concentration ratio at steady state based on brain homogenate method; $K_{p,uu}^{in vitro} = C_{u,brain} / C_{u,plasma}$

$AUC_{tot,brain}$: area under the concentration–time curve of the total concentration in brain

$AUC_{tot,plasma}$: area under the concentration–time curve of the total concentration in plasma

$AUC_{u,brainISF}$: area under the concentration–time curve of the unbound concentration in brain ISF

$AUC_{u,plasma}$: area under the concentration–time curve of the unbound concentration in plasma

$f_{u,plasma}$: *in vitro* fraction of unbound drug in plasma; $f_{u,plasma} = C_{u,plasma} / C_{tot,plasma}$

$f_{u,brain}$: *in vitro* fraction of unbound drug in undiluted brain (ISF + ICF); $f_{u,brain} = C_{u,brain} / C_{tot,brain}$

$C_{tot,plasma}$: *in vitro* total concentration in plasma

$C_{u,plasma}$: *in vitro* unbound concentration in plasma

$C_{tot,brain}$: *in vitro* total concentration in brain; $C_{tot,brain}$ = total amount of drug in blood-free brain homogenate divided by the volume of undiluted blood-free brain homogenate

$C_{u,brain}$: *in vitro* unbound concentration in brain (excluding blood) homogenate, determined by equilibrium dialysis

ISF: brain interstitial fluid; i.e., brain extracellular fluid not including blood

ICF: intracellular fluid

$t_{1/2,eq}$: half-time

PS: permeability surface area product

K_{in} : brain uptake clearance